7-7-2010

Modeling and Experimentation of Micro-Scale Self-Assembly Processes

Gary Hendrick
University of South Florida

Modeling and Experimentation of

Micro-Scale Self-Assembly Processes

by

Gary Hendrick

A thesis submitted in partial fulfillment
of the requirements for the degree of
Master of Science in Mechanical Engineering
Department of Mechanical Engineering
College of Engineering
University of South Florida

Major Professor: Nathan Crane, Ph.D.
Nathan Gallant, Ph.D.
Alex Savachkin, Ph.D.

Date of Approval:
July 7, 2010

Keywords: Assemblies, Micro-Integration, Capillary Forces, Stochastic Processes, Assembly Kinetics

ACKNOWLEDGEMENTS

This work was conducted in part through funding from NSF grant CMMI 092637 and with the help of James Tuckerman, Brian Bertram, Mario Juha, Sean Hollis and Nathan Crane, Ph.D.

TABLE OF CONTENTS

LIST OF TABLES

LIST OF FIGURES

Modeling and Experimentation for Micro-Scale Self-Assembly Processes

Gary Hendrick

ABSTRACT

Self-Assembly in the context of micro-scale integration refers to a developing set of techniques which exploit phenomena resulting in the spontaneous integration of micro-scale components into designed systems. Self-Assembly may be leveraged most effectively in parallel assembly processes. This thesis studies the modeling of micro-scale self-assembly processes as stochastic processes. The researchers propose that self-assembly processes may be modeled as Markov chains. In order to develop these models a Self-Assembly test system was created and trials were conducted using this system. Initial tests into the hypothesis that variables contributing to the transition probabilities include the kinetic energy of the assembly interaction, the energy minimized during assembly, and the area fraction of bonding sites on the assembly surface are tested.

CHAPTER 1: INTRODUCTION

The thesis presented here reports on work undertaken by the author in the University of South Florida's micro-integration lab. This work focused on the development of predictive models for micro scale self-assembly processes and the tools for verifying those models. Self-Assembly is a promising new method for micro and nano scale integration processes. The technology is not yet widely implemented in industrial processes and the majority of work in the field is in basic research. This thesis likewise focuses on basic research into self-assembly processes.

The following definition of Self-Assembly, can be found in John A. Pelesko's *Self-Assembly: The Science of Things That Put Themselves Together*: "Self-assembly refers to the spontaneous formation of organized structures through a stochastic process that involves pre-existing components is reversible, and can be controlled by proper design of the components, the environment, and the driving force."[1]

The term self-assembly may be applied to behavior at any scale and its characteristics are observed in a wide variety of systems. The

research presented here focuses on the assembly of mechanical components at the micro-scale.

1.1 Motivation

The case for the need for means to integrate micro-scale components through self-assembly is made by Morris, et al. [2]. In this work, the researchers synthesize data on assembly rates of various sized components in order to explore the relationship between component size and rate of assembly. They make the argument that the rate of assembly using traditional assembly methods finds its global maxima at roughly 300 μm. At this point component size has dropped to the point that inertial forces play a small part in the process. Assemblies conducted with traditional methods at this scale tend to result in simple 2D shapes.

The assembly rate decreases for components smaller than 300 μm, possibly due to a greater difficulty in grasping parts or to the relatively high inertia of the assembly mechanisms in comparison to the parts themselves. Figure 1-1 graphically represents Morris' results. The potential of self-assembly lies in the application of the technology to change the nature of the curve throughout the section indicated with the balloon "Self-Assembly contributes here …." This section indicates the region of the rate/size relationship which may be realized

through the development of Self-Assembly methodologies for micro-scale assembly.

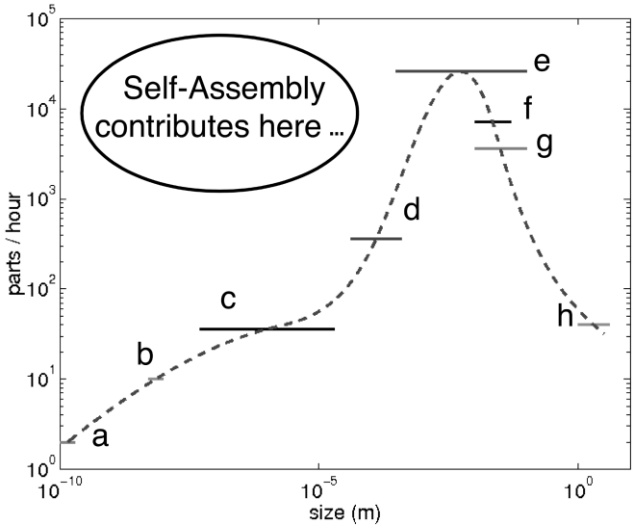

Figure 1-1: Assembly rate variations with component size.[2]

The widespread industrial application of self-assembly technologies requires that predictive models for the processes be developed. Through modeling, self-assembly processes may be accurately analyzed allowing process designers to effectively predict the behavior of these processes. With the maturation of self-assembly techniques, a wide range of constraints traditionally associated with modern robotic assembly processes will be lifted. The use of self-assembly techniques in electronics packaging specifically will have implications to the fabrication of semi-conducting devices allowing for improvements in a number of important performance parameters such as heat flux improvements due to new possibilities in the design of

component geometry and cost reductions due to reductions in loss of bulk material as component sizes may be reduced to take advantage of a greater capability to assemble components with smaller characteristic dimensions.

1.2 Scope

This thesis presents basic research into capillary driven self-assembly. Much of the work conducted throughout the course of the research period dealt with the development of the techniques required to run the self-assembly trials presented in the section "Results". These techniques include the application of surface treatments, the measurement of key process parameters, and the use of automation technologies to aid in the repetition of tests. This document itself reports on relevant background, modeling, preparation and experimentation with capillary driven self-assembly processes.

1.3 Outline

Chapter 1 of this document presents an introduction to the document, the motivations behind conducting this research and its scope.

The second chapter, Background, explores the prior art of modeling applicable to self-assembly. These models include those

adopted from chemical kinetics, surface energy modeling, and the modeling of stochastic processes.

Chapter 3, Proposed Model, contains a description of the novel model of self-assembly proposed in the thesis. The details of the stochastic model of the assembly system are presented along with a unit cell model describing the dynamics of individual interactions.

The fourth chapter presents the testing methods developed by the researchers along with the results of the tests used to validate the models. The methods section includes descriptions of the test apparatus developed for this system. The results include an analysis of the test results and comparison to model predictions.

The fifth and final chapter, Conclusions, includes both conclusions drawn from the thesis, and plans for future works to be accomplished at the USF micro-integration lab.

CHAPTER 2: BACKGROUND

Self-assembly is a broad topic. The application of self-assembly to micro-scale component integration may be achieved through the application of capillary forces to self-assembly. This chapter provides background necessary to understand the phenomena at work during the assembly processes under investigation, general data on the nature of self-assembling systems, and an exploration of prior art in the field.

2.1 Surface Tension

Surface tension occurs at the interface between two immiscible fluids or at the interface between a gas and a liquid. This tension is caused by unbalanced cohesive forces at the interface. Molecules at the surface of the fluid are subject to a net inward force while those within the fluid experience equal forces in all directions. These unresolved forces appear to create a hypothetical membrane at the interface which can be characterized by surface tension which has units of Force per Length and is designated by the Greek symbol sigma, σ [21]. This tension can be used in self-assembly processes to bind assembly components, and has been demonstrated to be useful

for such purposes [11, 14, 22]. These cases are discussed in greater detail below. First, a more complete description of the mechanisms behind capillary binding and surface energy minimization follows.

Due to surface tension, an interface develops pressure. This pressure can be used to determine the force at the interface. The force is balanced by the pressure differential between the internal and external pressures acting over the area of surface. For the spherical drop shown in Figure 2-1, the force at the edge of the drop is $2\pi R\sigma$. This force is balanced in the Equation 2-1.

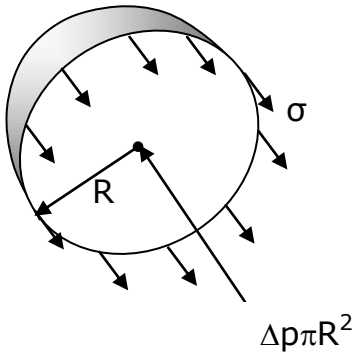

Figure 2-1: One half of a spherical liquid drop with forces.

$$2\pi R\sigma = \Delta p\pi R^2 \qquad \text{Equation 2-1}$$

Surface energy is the work associated with the interface through increasing the interface's energy by a unit area and is represented by the Greek symbol γ. Specific surface energy and surface tension are different terms for the same quantity and with the same magnitude. These quantities will be referred to as surface energy throughout this

document. When a fluid wets a surface through capillary action it seeks a minimum surface energy. Figure 2-2 shows a three phase diagram of an interface. This interface is in equilibrium when the conditions of Equation 2-2, Equation 2-3, and Equation 2-4 are met. In equilibrium the net forces along each interface are equal to 0.

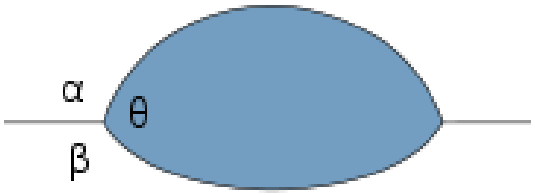

Figure 2-2: Three phases of fluid interface.

$$\gamma_{\alpha\theta} + \gamma_{\theta\beta}\cos\theta + \gamma_{\alpha\beta}\cos\alpha = 0 \qquad \text{Equation 2-2}$$

$$\gamma_{\alpha\theta}\cos\theta + \gamma_{\theta\beta} + \gamma_{\alpha\beta}\cos\beta = 0 \qquad \text{Equation 2-3}$$

$$\gamma_{\alpha\theta}\cos\alpha + \gamma_{\theta\beta}\cos\beta + \gamma_{\alpha\beta} = 0 \qquad \text{Equation 2-4}$$

This relationship can be simplified by setting the β phase in Figure 2-2 to that of a flat plane so that $\beta = \pi$, as is the case when a droplet is set upon a rigid surface. In the case that this model is applicable occurs the α-phase is a surrounding gas or immiscible fluid, β is the solid surface on which the droplet rests and θ is the contact angle of the fluid interface. This permits the three surface tensions and single contact angle to describe the interface. The resulting forces can be illustrated as shown in Figure 2-3.

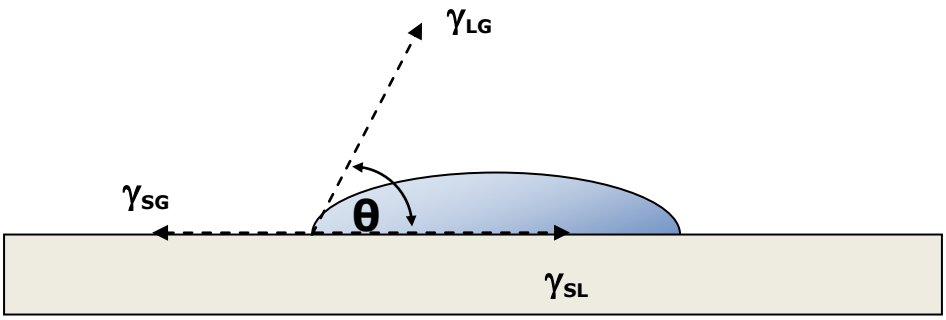

Figure 2-3: Young's law with planar geometry simplification.

$$\gamma_{SG} = \gamma_{SL} + \gamma_{LG}\cos\theta \qquad \text{Equation 2-5}$$

The Young-Dupre equation is shown in Equation 2-5 and is derived from Equation 2-3 using the above relationship for $\beta = \pi$. Within this relationship the contact angle of the fluid, θ, is used to describe wettability such that interfaces resting on a solid, rigid plane are wet if the fluid contact angle θ is less than 90°. In the case that the fluid is water, wettable solids are referred to as hydrophilic while non-wettable solids are referred to as hydrophobic.

2.2 Modeling Chemical Kinetics

Stochastic modeling for the dynamics of self-assembly processes presents a promising avenue toward developing useful modeling tools for industrial adoption of self-assembly processes. The application of accurate models to the design of self-assembling systems at the micro scale will aid process designers and self-assembly researchers to effectively scale successful self-assembly systems and to apply these

processes to new integration scenarios. The yield problem, defined as problem of predicting the final amount of complete bodies in an arbitrarily given self-assembling system [10], is an important question for the design of self-assembling systems. The exploitation of existing models for the purpose of answering the yield problem has been undertaken by several research groups. [4][5][10]

Many of the models adapted for application to self-assembling micro-scale systems were originally developed for the analysis of molecular structures. The problem of applying these models to micro-scale self-assembly has to do with adapting the molecular models to micro-scale systems. In a micro-scale application the legacy of the science describing bulk chemical processes are only tangentially applicable and for similar tools to become available in micro-scale self-assembly the basis of the process models must be revised. Some key differences which must be observed in scaling these processes up include a change in several order of magnitude for the concentration of reagents and the rate of reaction as well as large reductions in the complexity of shape and specificity in micro-scale parts as compared to their molecular analogues.

This section explores the scientific models used to describe chemical kinetics in order to identify the aspects of these models which are applicable to the kinetics of self-assembly at the micro-scale. An

exploration of rate equations for chemical reactions will provide the background for a review of several important studies.

A reaction can be represented with the notation:

$$aA + bB = cX \qquad \text{Equation 2-6}$$

Wherein the left side of the equation represents reactants and the right side of the equation represents products. The stoichiometric number for each component of the reaction is represented in the balanced equation above by a coefficient placed before the component symbol. The stoichiometric number for A in Equation 2-6 is a, for B it is b, and for the product X is c. The above notation also expresses the order of the reaction. The order of a reaction in respect to a reactant is the power to which that reactant is raise in the equation. The above reaction is a first-order reaction with respect to A, a first-order reaction with respect to B and it has the overall order of 2 which is found by summing the order of reaction for each reactants.

We may represent the rate of the reaction, v, as positive if the reaction moves forward, left to right in Equation 2-6, and negative if the reaction moves backward. Rate equations typically consider the concentration of reactants and products rather than quantities. This is accomplished by dividing both sides of the equation by the volume V, and these concentrations are represented by placing the component symbol in square braces. The rate of reaction v is negative for

products and positive for reactants and is equivalent to the rates of change of the concentration of each component divided by the reciprocal of the component's stoichiometric number. In the example above, these rates balance as follows in Equation 2-7.

$$\nu = -\frac{1}{a}\frac{d[A]}{dt} = -\frac{1}{b}\frac{d[B]}{dt} = \frac{1}{c}\frac{d[X]}{dt} \qquad \text{Equation 2-7}$$

The rate of the reaction may also be described through the use of a rate constant, k, and orders for the reaction signified by powers for the components of the reaction. The rate constant and the orders of the reaction with respect to each reactant must be determined experimentally. The orders of the reaction relative to the reactants are represented as α and β in Equation 2-8 and may take the form of any number and is not necessarily an integer.

$$\nu = k[A]^{\alpha}[B]^{\beta} \qquad \text{Equation 2-8}$$

It is clear that in chemical kinetics the rate of the reaction is dependent upon the order of that reaction. The order of the reaction with respect to A is expressed as α. The order of the reaction with respect to B is β. The overall order of reaction is equal to $\alpha + \beta$.

In the self-assembly studies concerned with kinetics which are examined later in this chapter only first-order reactions are considered. The following discussion of reaction concentrations over time and rate equations follows the development from Alberty [19].

A reaction of the form A -> products is a first-order reaction with the rate equation

$$-\frac{d[A]}{dt} = k[A] \qquad \text{Equation 2-9}$$

Integrating the preceding with t_1 taken to be 0 and the initial concentration represented as $[A]_0$ yields the following

$$[A] = [A]_0 e^{-kt} \qquad \text{Equation 2-10}$$

In order to better understand the effect of reaction order upon the rate it is helpful to compare this first-order reaction to a second-order reaction. A second-order reaction dependent upon the square of the reactant and taking the form $A \rightarrow products$ follows the rate law

$$-\frac{d[A]}{dt} = k[A]^2 \qquad \text{Equation 2-11}$$

Integrating the preceding with t_1 taken to be 0 and the initial concentration represented as $[A]_0$ yields the following

$$[A] = [A]_0 e^{-kt} \qquad \text{Equation 2-12}$$

A comparison of the concentration of reactants in the cases of first- and second-order reactions is illustrated in Figure 2-4.

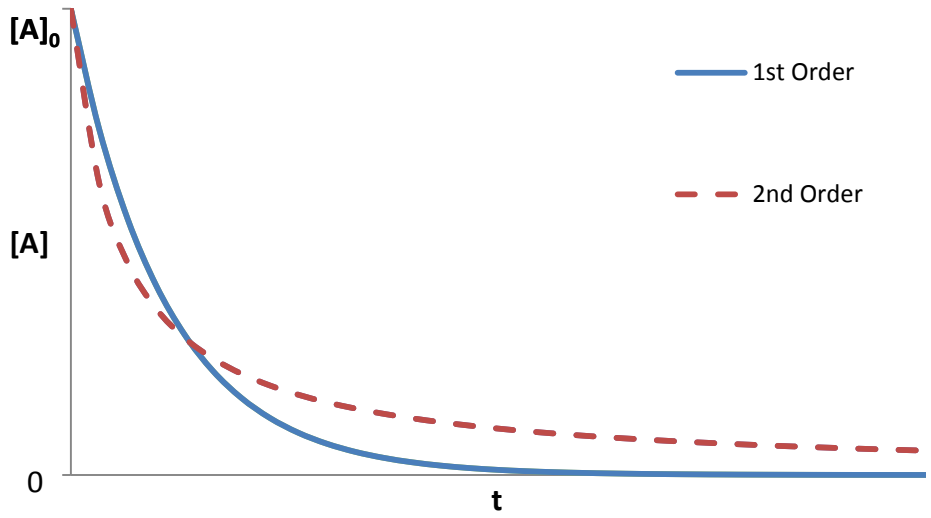

Figure 2-4: First- and second-order reaction rate laws.

In the case of a first-order reaction the rate of reaction ν is proportional to only the concentration of a single reactant i.e. $\nu = \mathrm{k}[\mathrm{A}]$. The rate constant, k, for the rate equation may be calculated by linearizing the plot of time vs. the concentration of the reactant and taking the negative of the slope of the line.

$$ln[A] = ln[A]_0 - kt \qquad \text{Equation 2-13}$$

In the case of a second-order reaction, the rate of reaction ν is proportional to the product of the concentrations of two reactants, or to the square of a single reactant. In the case of a single second-order reactant the rate equation will take the form below

$$\nu = -\frac{1}{a}\frac{d[A]}{dt} = k[A]^2 \qquad \text{Equation 2-14}$$

The rate constant for the reaction can be found through integration and rearrangement as in Equation 2-15.

$$k = \frac{\frac{1}{[A]} - \frac{1}{[A]_0}}{t} \qquad \text{Equation 2-15}$$

In the case of a second-order reaction in which the rate of reaction ν is proportional to the product of the concentrations of two reactants the rate equation is shown in Equation 2-16, and the rate constant can be shown to be equal to Equation 2-17.

$$\nu = -\frac{1}{a}\frac{d[A]}{dt} = -\frac{1}{b}\frac{d[B]}{dt} = k[A][B] \qquad \text{Equation 2-16}$$

$$k = \frac{\frac{1}{b[A]_0 - a[B]_0} ln \frac{[A][B]_0}{[A]_0[B]}}{t} \qquad \text{Equation 2-17}$$

Given these basic relationships for various reactions it is necessary to consider the methods by which the rate equation may be determined experimentally. The description of this procedure follows the treatment by Alberty pp. 625-637 [19].

For the reaction A + 2B = X, the rate equation takes the form seen in Equation 2-8 above, $\nu = k[A]^{\alpha}[B]^{\beta}$. In order to avoid complications in determining the rate due to the formation of the product X instantaneous rate measurements made before the product concentrations become significant and may be considered to be absent.

The process of determining the rate equation requires experimental data which, in the case of chemical kinetics, is often the result of successive measurements using methods such as light absorption to develop experimental points for $\Delta c/\Delta t$ And extrapolate that data back to t = 0. This data may be used to fit lines for the relationship [A] vs. time. If data on only the first 10% of the reactions are used, a linear regression to fit the concentration to the equation [X]/t = b + ct will be sufficient. The parameter b is the initial forward reaction rate of the reaction v_f. Using successive sets of measurements with variations in the initial concentration of the reactant in question $[A]_0$ will allow the relationship between $\ln v_f$ and $\ln[A]_0$. This relationship will reveal a slope equal to the order of the reaction.

The preceding tools from the study of chemical kinetics have been applied to the study of micro-scale self-assembly [4][5][10][11]. This will be addressed in greater detail in the section entitled "Application of Chemical Kinetics to Self-Assembly".

2.3 Prior Art

Micro-Scale Self-Assembly has been studied for some time and demonstrations of the application of self-assembly processes have been conducted in an experimental setting and recently in a

commercialized process by Alien Technology Inc. The body of work available for review in literature includes a number of demonstrations of self-assembly for micro-scale integration as well as a several techniques for modeling these processes. These previous efforts are described below.

2.3.1 Demonstrations of Self-Assembly Processes

Parallel fluidic self-assembly on the micro-scale has been explored extensively over the course of the past two decades. Demonstrations of self-assembly processes have typically accompanied exploration of the underlying principles of self-assembly. The techniques applied in these processes will be discussed immediately and the importance of their underlying principles will be covered in following sections.

One of the earliest explorations of micro-scale self-assembly was conducted by Yeh, et al. who demonstrated a technique in which GaAs light-emitting diodes were fabricated with a shaped features were introduced into a fluidic transport and washed over a silicon substrate containing complimentary shaped binding sites to control position and orientation [3, 4]. This work reported a 90% fill ratio for the holes while immersed in carrier fluid, but degradation after evaporation due to surface tension reduced the yield to a fill ration between 30 and 70

percent. This degradation in total yield is a direct result of relying exclusively on gravity, a relatively weak force at this scale, to fix parts into place. The gravitational forces were easily overcome by capillary forces during the drying process causing many parts to shift out of their previously stable positions.

Yeh referred to the process combining fluid transport and shape recognition between part and substrate as Fluidic Self-Assembly (FSA). A later study from the same researcher group, authored by Ashish Verma, provides a formal definition of FSA as follows.

"[Fluidic Self-Assembly] involves the placement of devices fabricated onto specifically-shaped structures ("blocks") of one material into similarly shaped receptacle holes made on a substrate of some other material."[5]

FSA remains an important method in self-assembly and has been improved upon and used successfully in numerous research endeavors exploring both modeling of self-assembly and the techniques and methods necessary to implement self-assembly industrially [3-9]. The initial explorations into FSA included trapezoidal parts and holes which required novel fabrication processes. This would limit the ultimate applicability of the FSA process as any self-assembly process must consider the integration of parts fabricated using traditional methods.

2.3.2 Modeling Self-Assembling Systems

The exploration of self-assembling behavior for the micro scale has led to a number of important observations. Simple mechanical assembly models conducted in two dimensions have been used for these purposes by Hosokawa, et al. whose 1999 work "Dynamics of Self-Assembly Systems: Analogy with chemical kinetics" [10] is explored in greater detail below in the "Modeling Chemical Kinetics" section of this thesis. In this work solid triangles were vibrated on a surface and the emerging assembled structures were observed and used to validate a predictive model of the yield of the process. Hosokawa again employed these methods in 1999 to describe the behavior of a two-dimensional self-assembly for parts on a liquid-air interface in which the parts were fabricated with a curved feature which controlled the size of the parts' menisci [11]. In that study, Hosokawa also explored the effect of menisci upon assemblies at a liquid-liquid interface, demonstrating that parts with similar shapes but dissimilar menisci were mutually repulsive.

The study of the two dimensional assembly at the interface between fluids and the behavior of components at these interfaces has been explored by other research ventures. The practice of controlling individual properties of otherwise shape identical assembly components has been successfully applied in several demonstrations of

two and three dimensional assembly at interfaces. These techniques are capable of providing control over the shape and behavior of integrated structures of shape identical parts through the application of surface property patterning.

The Whitesides group, working out of the Department of Chemical Biology at Harvard University, has applied such principles in several noteworthy cases. In 1999 they published works regarding the two-dimensional self-assembly of micro-scale components at a liquid-liquid interface between an organic liquid and an aqueous liquid [12, 13]. In both studies, they explored the potential of using capillary forces to act as a "bond" between self-assembling components, and how variations in the bonding forces and the interaction environment affect the assembly structures. In order to mimic the behavior of biological systems in which specificity is governed by shape recognition and hydrophobic patterning they varied the patterning of hydrophobic-hydrophilic areas on the assembly components, the shape of the menisci at the edges of the parts through variations in density or surface energy of the part surfaces, and the densities of the three interacting phases of the organic liquid, aqueous liquid and polymeric solid. These studies demonstrated how complex behavior can arise out of small variations in a limited set of building blocks [12, 13]. In 2003, this laboratory continued its work on the application of capillary

interactions through an exploration of interactions of hexagonal plates at a liquid-liquid interface self-assembling into two-dimensional arrays [14]. Again, the components of the assembly were shape-identical PDMS hexagons, they were prepared with five different permutations of hydrophobic and hydrophilic faces, and they were doped with varying degrees of aluminum oxide in order to affect their density and thus the shape of their menisci. This work compliments the 1999 [12, 13] work completed with similar parts but adds the complexity of having both positive and negative menisci associated with the assembly.

Work such as that described above has continued to influence the development of principles such as shape, and pattern recognition in self-assembly. The Whitesides group has since continued to develop its work and extend their exploration of the principles of self-assembly to observe new phenomena. In the year 2000 they published work on the three dimensional self-assembly of micro-scale hexagonal rods [15]. This research continued to apply capillary forces as the "bonds" between self-assembling components. This new work is similar to previous studies in that it shares the quality of exploring the behavior of parts fabricated identically and agitated within a self-assembly environment in order to express complex final structures through variations in surface properties. As demonstrated with the studies of

hexagonal plates at a liquid-liquid interface [12, 13], this study successfully demonstrated a single shape of building block expressing numerous final structures with differences in size of section, structure, and stability. Furthermore, alignment of the parts through capillarity was also observed, a strategy exploited in many capillary driven self-assembly processes.

This work has continued to develop into further studies of the effect of capillary forces on the shape and structure of 3D micro-scale assemblies through self-assembly processes. In 2002, more complex 3D structures were integrated through self-assembly including a helical electrical circuit modeled after the tobacco mosaic virus. In this study the researchers developed strategies for applying varied surface properties to control complex structures out of shape-identical parts. The focus in this case was to explore systems of orthogonal interactions in which the driving force for assembly was a capillary force from one of two interactions caused by the coalescing of either perfluorodecalin, PFD, or a molten solder, the pair of which do not interact with one another [16].

The group conducted research published under "Fabrication of a Cylindrical Display by Patterned Assembly" [17] in which they depart from the liquid-liquid interfaces with lateral capillary action and instead assembled components onto a non-planer substrate using low-melting

point solder on the binding sites to act as both electrical and mechanical connections first to a lower electrode, then to a wafer of similarly patterned sites on an upper electrode. The process used first a set of 113 LEDs agitated in a bath with a cylindrical substrate onto which the LEDs fully assembled. The researchers then coated the top of the LEDs with solder and patterned solder to binding sites on a film containing the top electrodes for the assembly. The entire assembly was heated again after hand placing the two sides in contact and the upper electrodes were bound to the assembled LEDs on the lower electrode successfully. The same procedure was applied to a larger assembly in which 1600 receptors and silicon blocks were assembled similarly with 98% coverage and an alignment accuracy of ~3° and was completed in roughly 3 minutes. These assemblies illustrate strengths of self-assembly including the speed of process through parallel self-assembly and the capability to assemble functional non-planar assemblies.

The detailed descriptions of modeling and process design included in the cited literature are representative of the state of the art in research, and many of those processes include statistics for rate of assembly and other performance parameters in processes conducted as proof of concept. The Alien Technologies process is not available for review however, according to Mastrangeli, et al. the company claims

that its process is capable of assembling roughly two million parts per hour [18]. This claim is very promising, however lacking published literature the author will focus upon the well documented applications of self-assembly conducted experimentally along with the published modeling techniques referenced above.

2.3.3 Application of Chemical Kinetics to Self-Assembly

Process parameters such as rate constants and order of reaction, well-developed in the study of chemical kinetics, need renewed exploration if they are to be applied to the study of micro scale self-assembly. The application and demonstration of kinetic models to self-assembly processes started with Verma et al. who conducted their experiments using a Fluidic Self-Assembly (FSA) environment in which part-to substrate SA systems were applied to test a rate equation model [5].

The researchers in Verma, et al. 1995, were concerned with developing a set of rate equations using a steady-state model in which the availability of parts and substrates is non-diminishing. The work of Verma represents a first-order system and was validated experimentally using a system which re-circulated parts over a substrate patterned with holes into which parts could bind given a shape match. The nomenclature for this experiment follows:

R_1	Rate of Assembly
R_2	Rate of Disassembly
C_1	Assembly Constant
C_2	Disassembly Constant
N_b	Number of blocks
n_b	Number of blocks left in Solution
N_b	Number of Holes
n_h	Number of Unfilled Holes
f	Number of Filled Holes
K	Associativity Ratio $\frac{C_1}{C_2}$
x	Fill Ratio

These constants and parameters can be arranged algebraically to express the following relationships in which the rate of assembly and the rate of disassembly are leveraged to determine the fill ratio.

$$R_1 = C_1 n_b n_h \qquad \text{Equation 2-18}$$

$$R_2 = C_2 f \qquad \text{Equation 2-19}$$

When the assembly reaches equilibrium the rate of assembly is equal to the rate of disassembly and the following equivalence is found.

$$C_1 n_b n_h = C_2 f \qquad \text{Equation 2-20}$$

This equation can be rearranged as follows to find the fill ratio at equilibrium. In practice, this relationship would need to be used in

order to ensure that the fill ratio is sufficiently close to 1 resulting in the assembly operating as expected.

$$x = \frac{Kn_b}{1 + Kn_b}$$ Equation 2-21

The fill ratio, x, can be effectively manipulated to reach 1 by increasing either K or n_b. In the thesis work, we capitalize upon this relationship by reducing C_2, the probability that a hole will become unfilled, through manipulation of the surface energy to kinetic energy ratio involved in the binding process for the assembly process. This facet of the research is explored in greater depth in later chapters.

The application of the chemical kinetic analogy is continued in the work of Hosokawa et al. with the intention of developing analogous yield and rate equations for micro-scale systems and to clarify the dynamic evolution of self-assembling systems [1].

Hosakawa's analogy includes a clear procedure for the application of his model to an assembling system. In this procedure the experimenter begins with a number of parts which may assemble with one another in multiple manners. The concentration of every intermediate product is a state variable. This reduces the degree of freedom of the system by forcing the model to only consider the stable intermediate products. After deriving the dynamics governing the state variables from the constraints of the processes being explored the variation of the states may be calculated.

In Hosokawa, et al. 1996, a set of state variables, representing the intermediate products of the assembly process is defined as X_1, X_2, X_3, X_4. The states considered in that research are states representing the integration of parts floating at a fluid interface into two-dimensional structures. These states are illustrated in the following figure.

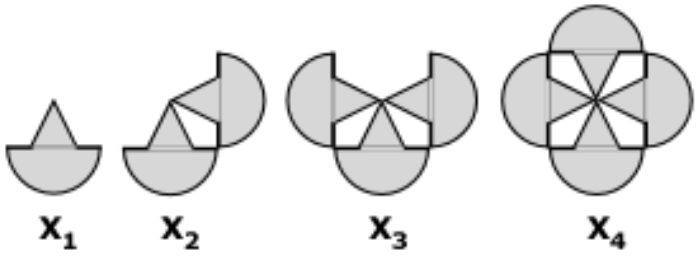

Figure 2-5: Possible assembly states for Hosokawa study.
The number of assemblies in state is represented as x_i.

Time in this case is represented as a time step t which occurs at each collision of clusters. So that the number of assemblies in any state is altered at a collision according to

$$\boldsymbol{x}(t+1) = \boldsymbol{x}(t) + \boldsymbol{F}(\boldsymbol{x}(t)) \qquad \text{Equation 2-22}$$

Where $\mathbf{F} = F_1, \ldots F_n$.

F_i represents the number of additional assemblies in state Xi after a collision, and can be represented as the sum of the products of $v_{ij}P_j$. Where, v_{ij} is stoichiometric number for the reactions producing Xi

and P_j is the probability of the jth reaction occurring given the current state of the system.

$$F_i = \sum_j v_{ij} P_j \qquad \text{Equation 2-23}$$

$$P_j = P_{\text{im}}^{\,b} P_{\text{im}}^{\,c} \qquad \text{Equation 2-24}$$

The quantity P_j is a product of two other probabilities explored in greater depth in the thesis work, the probability of a reaction collision occurring and the probability of a reaction bond being formed, $P_{\text{im}}^{\,b} P_{\text{im}}^{\,c}$. Their work concluded that the state of the self-assembling systems can be used as state variables in stochastic analysis and that chemical kinetics and population dynamics can provide useful analogies for the self-assembly of systems. The researchers use Hosokawa's work in order to explore the means by which the probability of bonding, given a collision, can be made to approach 1, certainty. Avenues toward guaranteeing that the bond is formed are pursued through the exploitation of the relationship between the bond energy of a stable bond and the kinetic energy of a part and site in collision. By ensuring that the kinetic energy of the collision is low relative to the bond energy of an assembly a bond can be expected to form upon collision.

CHAPTER 3: PROPOSED MODEL

The following chapter presents the proposed model for this research. The modeling is conducted in two parts. The system model presents a Markov chain model of the parallel assembly method. The Unit-cell model explores the dynamics of the assembly process.

3.1 System Model

The model developed in this thesis concerns itself with the evolution over time of a self-assembly process. This model observes a state space in which assembly components may be exist in different states of assembly, i.e. assembled, unassembled, misassembled, etc. The individual states of the assembly process are represented by a set of random variables denoted by the vector X. The evolution of each state $\mathrm{X_i(t)}$, evolving over time, represents the number of assembly parts which have entered state i at time t. This collection of random variables evolving through time represents a time-dependent stochastic process [20].

For the purposes of modeling this stochastic system let the vector of random variables $\mathrm{X} = \{\mathrm{X_n}, \mathrm{n} = 0, 1, 2, \cdots\}$ represent the state space for the process. The process is said to be in state i at time step

n when $X_n = i$ [20]. The model considered in this research includes just two states for the assembly. These are states X_0, which represents an unbound part, and X_1, in which a part is bound to an assembly site.

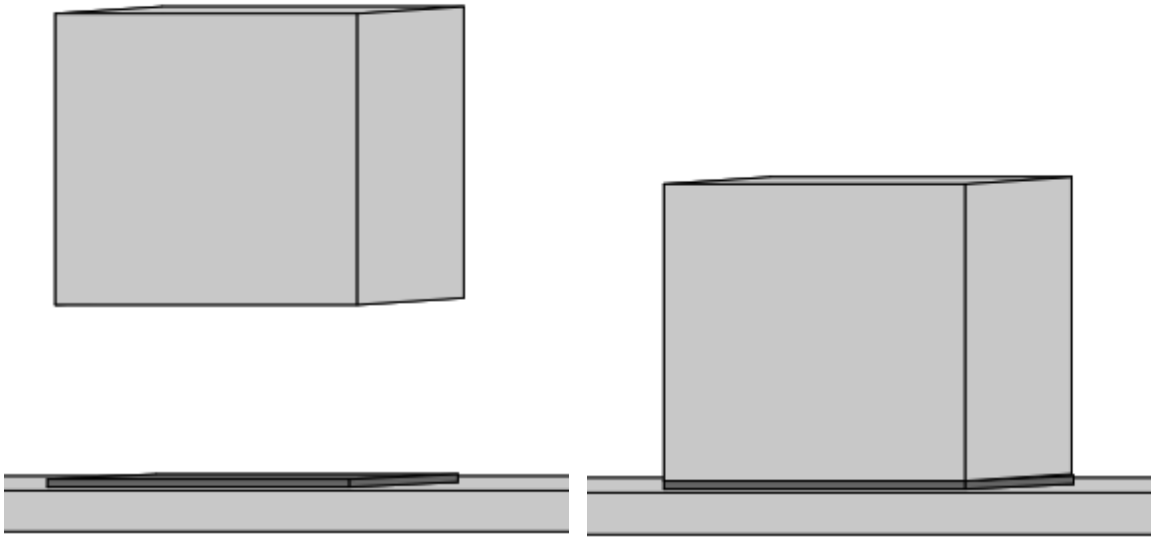

Figure 3-1: The two assembly states of the proposed model. These include state X_0 for unassembled parts on the left, and X_1 for assembled parts on the right.

A stochastic process in which the conditional distribution of any future state is dependent upon only the present state is known as a Markov Chain. In the case of a Markov Chain, there is a fixed probability, P_{ij} that the process will move from state i to state j. This statement can be expressed formally in Equation 3-1.

$$P\{X_{n+1} = j | X_n = i, X_{n-1} = i_{n-1} \ldots X_1 = i_1, X_0 = i_0\} = P_{ij} \qquad \text{Equation 3-1}$$

A one-step transition matrix, $\boldsymbol{P}$, is composed of all probabilities of transition from i to j for all states within the state space **X**.

$$P = \begin{Vmatrix} P_{00} & \cdots & P_{0m} \\ \vdots & \ddots & \vdots \\ P_{n0} & \cdots & P_{nm} \end{Vmatrix} \qquad \text{Equation 3-2}$$

For such a transition matrix, the following properties hold

$$P_{ij} \geq 0; \qquad i,j \geq 0; \qquad \sum_{j=0}^{\infty} P_{ij} = 1; \qquad i = 0,1,\cdots \qquad \text{Equation 3-3}$$

The statements of Equation 3-3 must be true.[20]

3.1.1 Simulation of Stochastic Processes

A Monte Carlo simulation may be used to approximate solutions for the expected value of a function operating upon the state space of a stochastic process. In general, if the state space X denotes a random vector having a density function $f(x_1 \ldots . x_n)$ the expected value of an n-dimensional function g, may be approximated by solving the multiple-integral from Equation 3-4.[20]

$$E[g(\boldsymbol{X})] = \iint \cdots \int g(x_1, \ldots, x_n)\, f\left(x_1, \ldots, x_{\{\{\}\}n}\right) dx_1 dx_2 \ldots dx_n \qquad \text{Equation 3-4}$$

In situations in which it is difficult or impossible to solve Equation 3-4, it may be possible to approximate a solution to the system by means of a Monte Carlo Simulation. A Monte Carlo Simulation makes use of the strong law of large numbers to generate an average for the expected value of the n-dimensional function g. This is done by generating random vectors $\boldsymbol{X}^{(i)} = \left(X_1^{(i)}, \ldots, X_n^{(i)}\right)$ having the joint density function $f(x_1 \ldots . x_n)$. For each value of $\boldsymbol{X}^{(i)}$, compute

$Y^{(i)} = g(\boldsymbol{X}^{(i)})$. After having generated r, a fixed number of independent and identically distributed random variables for this formulation with, $i = 1, \dots, r$ an approximation of the solution Equation 3-4 can be found as in Equation 3-5[20]

$$\lim_{r\to\infty} \frac{Y^{(1)} + \ \dots + Y^{(r)}}{r} = E\left[Y^{(i)}\right] = E[g(\boldsymbol{X})] \qquad \text{Equation 3-5}$$

3.1.2 Subject Model

The assembly model considered in this study accounts for a state space including parts in a state space consisting of assembled and unassembled parts. These parts are free parts which are introduced into an assembly environment and bound to an assembly substrate wherein the parts find a stable state.

X_0	Number of parts in a free state
X_1	Number of parts in an assembled state

The assembly process is initiated with all parts and sites in the free state and the values of the vector of random variables $\mathrm{X} = \{\mathrm{X}_0, \mathrm{X}_1\}$ evolves through time as a stochastic process as assembly proceeds. Let P_a represent the probability of transition from state 0, free, to state 1, assembled, indicates that a free part has encountered a binding site and successfully bound to it. Let a transition from state 1 to state 0, in which a part would undergo a disassembly from a previously bound

assembly site, be represented by P_u. The process is represented by a Markov chain with the following one-step transition matrix.

$$P = \begin{Vmatrix} 1 - P_a & P_u \\ P_a & 1 - P_u \end{Vmatrix} \qquad \text{Equation 3-6}$$

This process model can be seen in Figure 3-2, consisting only of two states. This model does not account for the possibility of bonding errors. As a first step, this research seeks to determine a method for predicting P_a. In order to facilitate these measurements, a system in which the probability of disassembly , P_u, is minimized will be used.

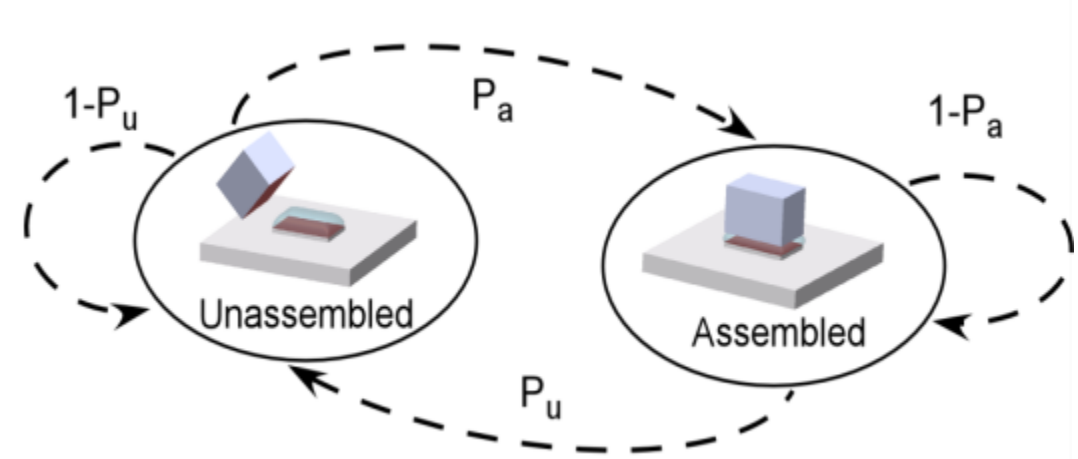

Figure 3-2: An illustration of the proposed Markov chain model. This models the interaction of assembly for a part to site.

In order to design the assembly process to allow for an absorbing state of assembly it is necessary to consider the dynamics of the interaction and develop a method by which the assembled state can be guaranteed to persist.

3.2 Unit Cell Modeling

3.2.1 Modeling of Assembly Dynamics

The researchers employ what we refer to as unit-cell analysis. This is a method of self-assembly process modeling on the basis of the dynamics of individual state transition interactions. The unit cell is depicted in Figure 3-3.

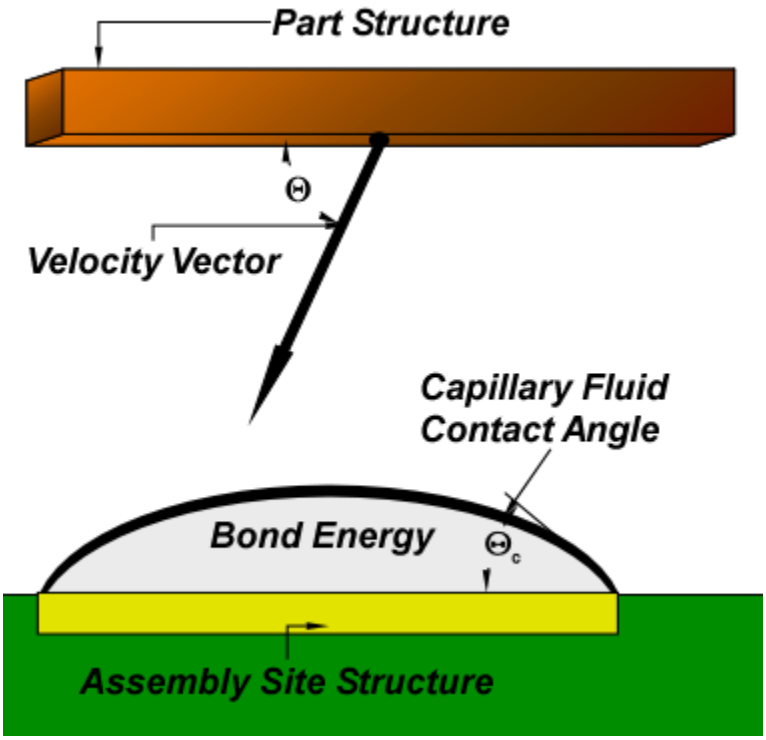

Figure 3-3: The assembly unit cell. This cell depicts process parameters important to the characterization of the assembly process.

This form of analysis depends on accurate characterization of the dependence of the transition probability on the physical parameters of the system. This "unit cell" is the interaction between one part-site pair. In the case of part to substrate self-assembly driven by

gravitational forces and bond through capillary forces, the unit cell interaction takes place as a part collides with a binding location.

Analysis of parallel self-assembly processes benefits from the analysis of global parameters affecting the dynamics of the unit-cell. The stochastic self-assembly process output is determined in part by the probability of binding after a successful collision has occurred. The thesis work explores how parameters such as bond strength and speed of approach during binding determine the transition probability of assembly. Accurate models require that controllable process parameters and their transition probability be effectively analyzed.

CHAPTER 4: SELF-ASSEMBLY TEST SYSTEM

In order to test and validate models for specific assembly processes it is necessary to control parameters contributing to assembly performance. In order to do so efficiently a test system was developed for application to the assembly process. This system allows the researchers to vary specific parameters of the assembly process and report on assembly yield.

4.1 Requirements

The requirements for the test system include spatial regularity and control over the energy involved in reactions.

The sites must be fixed within an assembly environment in order to guarantee the repeatability of the experiments. The parts must be introduced in a repeatable manner. These constraints guarantee the spatial regularity of the process.

The control over the energy involved in the reactions requires control over both the kinetic energy of an interaction and the bond energy of a finished assembly. The magnitude of the kinetic energy involved with the assembly interaction must be controllable. The exploration of the ratio of kinetic energy involved in an interaction to

the bond energy of an assembled set is a key process parameter explored throughout this research. The bond energy of an assembly must be controllable within the assembly environment. Within this system, this is achieved through the customization of surface properties for parts and sites and through the selection of bonding fluids.

4.2 Methods

In order to design self-assembling systems it is important to understand the complexity of the processes at work in the phenomena leveraged in these systems. A proper understanding of these processes may be used to inform stochastic models of self-assembling systems working at the micro-scale. Assembly interactions in such systems will include multiple interaction steps conducted with a variety of conditions. In capillary self-assembly, these conditions will include arrival angles and varied interaction activation and bonding energies. This diversified set of assembly conditions results in a large and varied set of "unit cell" behavior. Experiments designed to understand these behaviors must allow control of at least some of these process parameters. Independent control of these process parameters allow for the characterization of these processes.

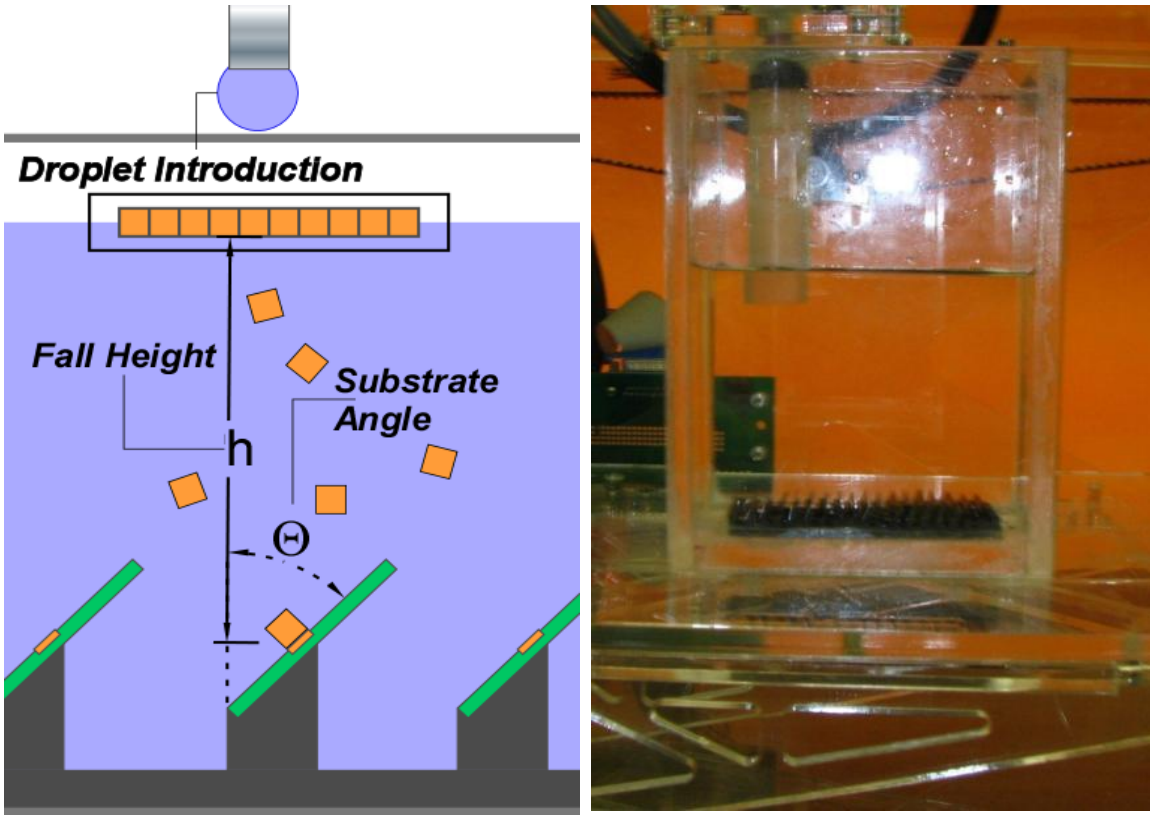

Figure 4-1: Assembly environment. The diagram on the left depicts the process parameters controllable through the assembly environment.

The labeled process parameters from Figure 4-1 include height of the free fall of parts introduced to the assembly environment and the angle of approach of these parts. Other controllable parameters include the spatial distribution of parts, the constitution of the fluidic assembly environment, and the pattern of available assembly sites within the environment. The selection of fluid will affect the surface energy of the assembly bonds. Furthermore, the viscosity of the fluid will alter the velocity of falling parts which controls the kinetic energy of the parts at the time of the reaction. Many other parameter alterations are possible within the assembly environment. The means

by which these variables can be controlled are enumerated in the following sections along with an account of an experiment making use of this test platform.

4.2.1 Test Apparatus

In these experiments, free parts are introduced into the assembly environment through the fluid-gas interface. Parts are placed on the fluid-gas interface where they remain unless agitated to fall through the interface. This is a function of the scale of the parts and the surface tension of the environmental fluid. In order to pass through this interface it is necessary to agitate the parts. This is accomplished through dropping fluid onto the floating parts using an automated syringe pump. The syringe pump is attached to a Fab@Home system, which provides planar actuation of the pump over the surface of the fluid. Because the location of the syringe is controlled and the rate of droplet introduction is also controlled the parts can be induced to enter the environment in a patterned manner.

As a droplet strikes parts on the surface they are forced parts fall into the assembly environment in a Gaussian distribution. Analysis of the assembly system relies on an ability to model the distribution of parts, which is better accomplished with a uniform distribution rather

than a Gaussian. A pseudo-uniform distribution is simulated by overlapping the individual Gaussian distributions.

Given a uniform distribution of parts the probability of a collision occurring is equivalent to the area fraction of the sites distributed over the assembly field. Only through this pseudo-uniform distribution can probability of assembly's probability of collision be considered equivalent to the area fraction of sites. As shown in 4-2 the pseudo-uniform distribution can be in good agreement with a truly uniform distribution.

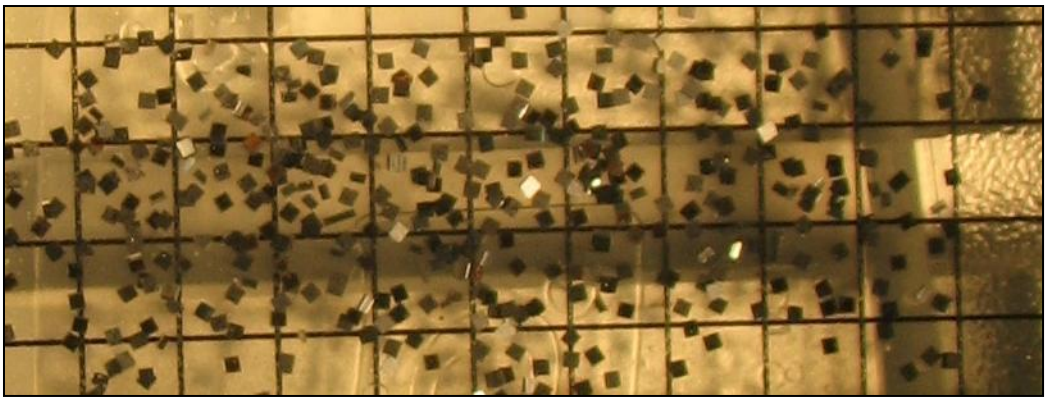

Figure 4-2: Distribution of random parts after introduction. Two rows of parts were dropped horizontally over a 2.5" width. The grid lines above are spaced at 0.25 inches.

4.2.2 Assembly Site Mount

The assembly sites for this platform are fixed at the base of the assembly environment on a substrate mount, the latest version of this mount is shown in Figure 4-3. The original version of the mounts are shown in Figure 4-4.

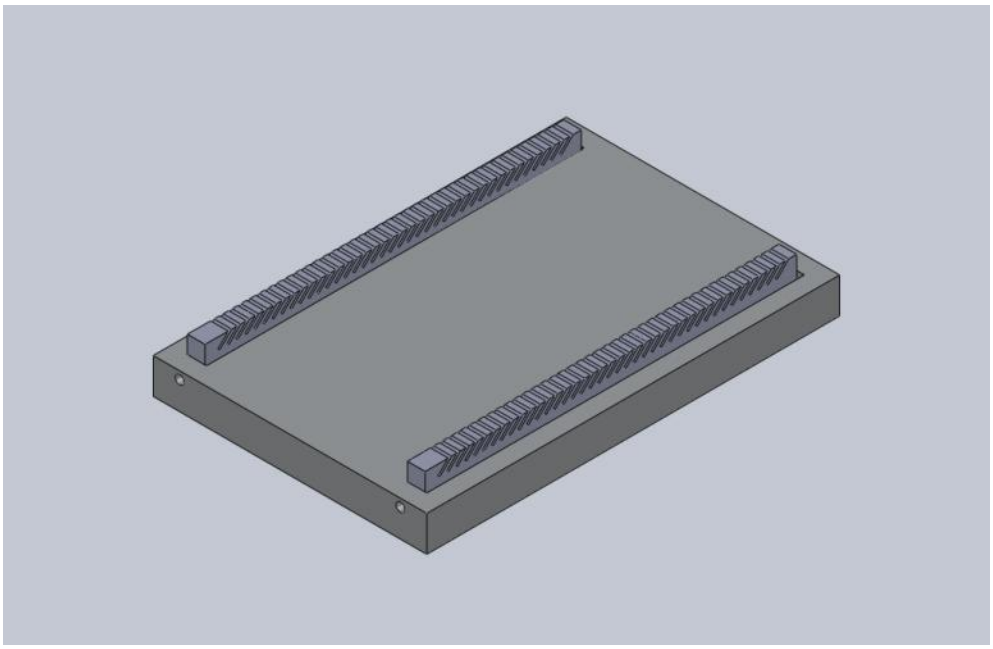

Figure 4-3: Assembly mount. The geometry of the mount dictates the area fraction of assembly sites within the assembly environment.

Through experimentation with the original mount design shown below, it was determined that the original design lacked flexibility and provided some obstacles to experimental setup which were addressed in the final design. Important improvements to the design include the use of slatted shelves rather than solid pedestal mounts. The slats allow sites to be pushed into place without overconstraint. The long shelves from the original design left sites subject to dislodging and required a high degree of manual dexterity to place the sites on the mounts. In both cases the mounts allow the sites to be spaced far enough from one another to permit parts which do not bind successfully to fall away into voids away from the assembly area.

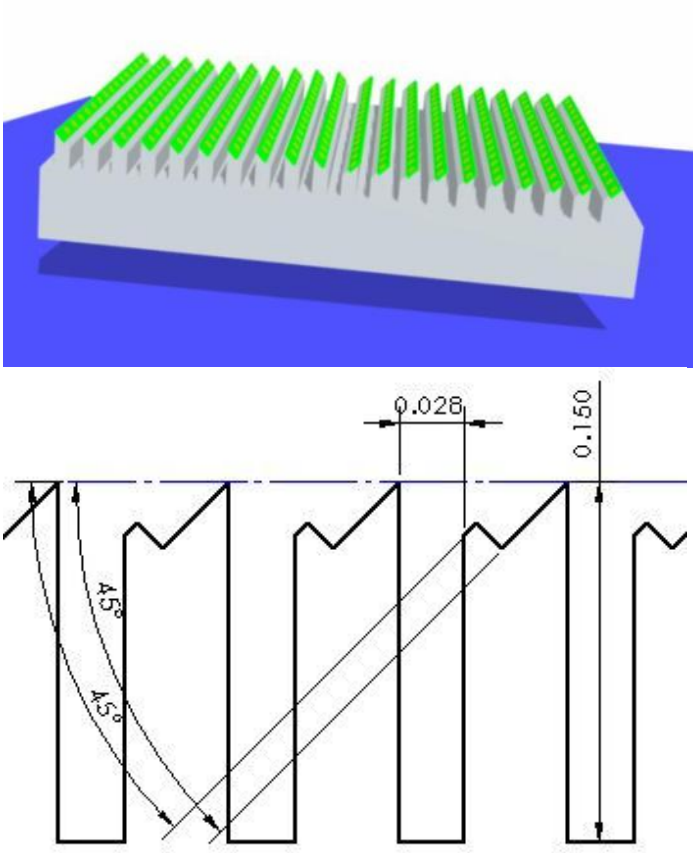

Figure 4-4: Original design of assembly mount. This milled aluminum sock holds sites in place at a 45° angle resting on shelves shown in detail on the bottom with dimensions in inches and degrees.

Mounting these sites provides a measure of control over several process parameters. The fixed location of the sites provides a constant fall distance for free parts dropping from the fluid surface. The terminal velocity of the falling parts is controlled through the viscosity of the fluid, the shape and size of the parts, and the density of the parts. This allows the researchers to set upper limits to the interaction kinetic energy for the assembly. Furthermore, the area fraction of assembly sites is an important characteristic of the

environment. A uniform distribution of parts over the substrate mount will interact with sites with a probability equal to the area fraction of sites distributed over the mount. Finally, the angle of the substrate mount surface can be varied by machining new mount shelves. This angle affects the arrival direction of the parts to the sites as well as the area fraction of sites exposed to the part distribution. Complete drawings of the assembly mounts can be found in Appendix A.

The parts are introduced through the air/fluid interface at the surface of the environmental fluid, a solution of Glycerol and water. As they fall they spread so that they land in a Gaussian distribution centered below the point at which they pass through the interface. In order to ensure that each binding site has a common likelihood of experiencing an assembly event, the drop point of the particle is varied over the surface of the fluid to provide a uniform distribution. With a uniform distribution the number of potential interactions is proportional to the area fraction of sites normal to the trajectory of falling parts. This ratio is a function of the patterning of binding sites as well as the angle of the substrate mounting. The function depends upon the patterning of the sites, however, given that A_s represents the area fraction of substrate area covered in active assembly sites, θ represents the angle of the substrates to the direction of travel of parts, and A_T represents the total area over which the parts are

distributed the area fraction, A_f, exposed to site interactions can be expressed with the following equation.

$$A_f = \frac{A_s \times \cos(\theta)}{A_T} \qquad \text{Equation 4-1}$$

The patterning of the binding sites must account for the interactions which will occur during assembly. It is important to space the sites far enough from one another so that a single part cannot span the empty space between sites. If such a binding were to occur its state would need to be accounted for in the state space of the assembly process. Figure 4-5 parts assembled to two strips of the patterned assembly sites.

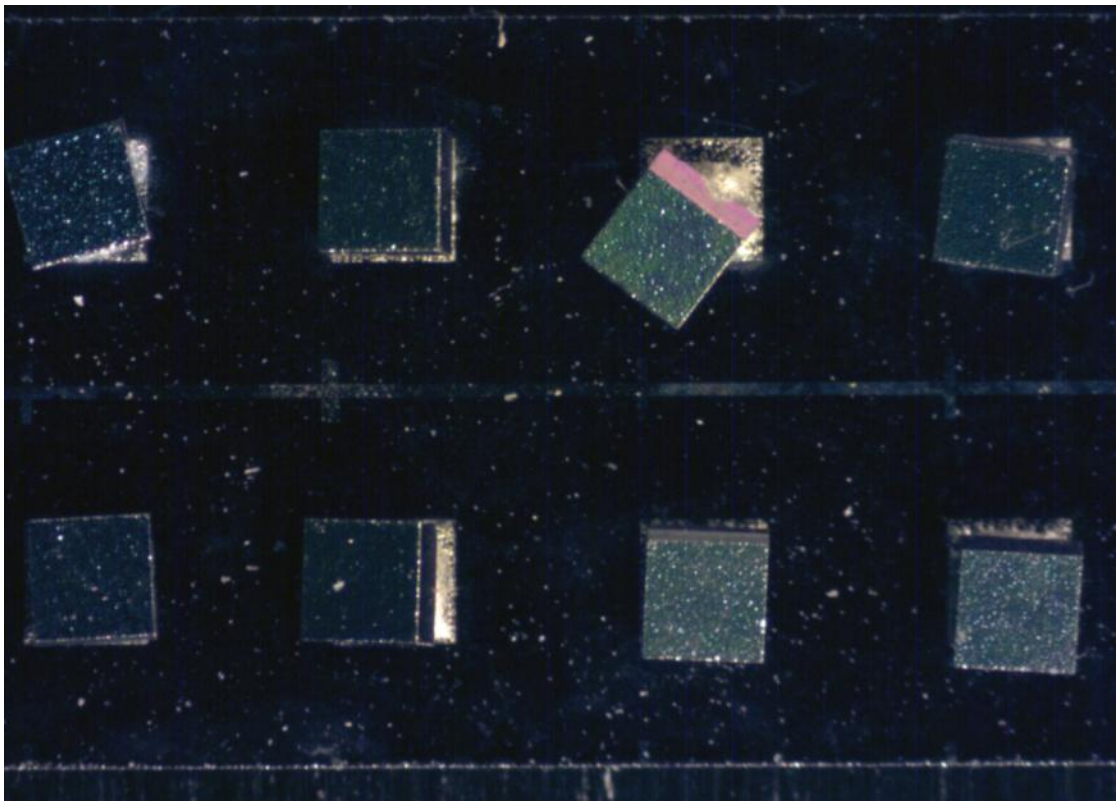

Figure 4-5: Sites with assembled parts. This assembly was conducted through manual placement of the parts onto the sites using a pipette to move parts into position. Note that the top row misalignment does not interfere with neighboring assemblies. Figure 4-5 illustrates the important dimensions of the site patterning.

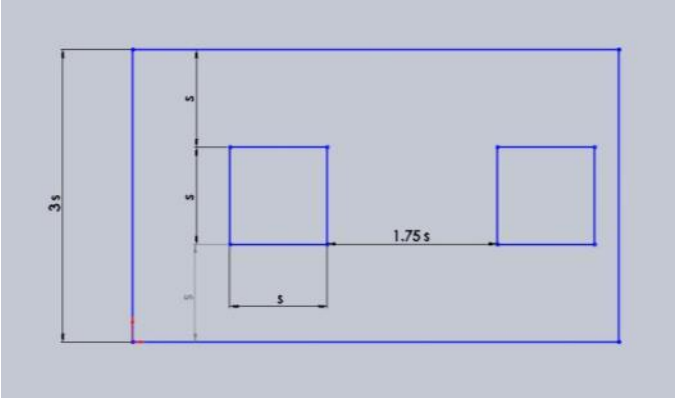

Figure 4-6: Site pattern schematic. Note that the square sites of side s are spaced at 1.75 s in distance to one another. This allows the cube sites to fall at their longest dimension between sites without interfering with more than one site.

4.2.3 Active Face Fraction

The effects of the site and part fabrication upon the bond energy and the kinetic energy for a unit assembly are described in greater detail in the following sections. However, it is necessary also to consider the significant effect of part shape upon bond probability in order to use the unit-cell model to effectively inform the stochastic model of the system. The initial requirement for an assembly process to occur begins with the activation of the assembly interaction. This occurs when the part physically encounters the site, the probability of which is dependent upon the area fraction of sites available for interaction as discussed previously. However, in the case of capillary driven self-assembly, it is necessary to consider that the orientation of the part upon entering the interaction is also important. The active fraction of the part's surface, the portion which will bond to an assembly site through surface energy minimization, has a direct effect upon the probability of assembly.

The researchers propose the hypothesis that the geometric contribution of a part's structure to the probability of an assembly interaction occurring during the assembly process is equivalent to the probability that the part be oriented correctly at the time of the interaction to bind to an assembly site. This probability defines the geometric limit of assembly. As shown in Figure 4-7 and Figure 4-8 the

geometric contribution the probability of assembly is considerable. For a sphere in which the entire surface is an active assembly site this contribution is 1. For a long thin plate with only one active site the contribution would be 0.5. For a cube with one site valid for assembly, as used in the experiments to follow, the contribution is 1/6. This geometric based limit to assembly is multiplied by the area fraction of sites within the assembly area to generate the probability of an assembly interaction occurring.

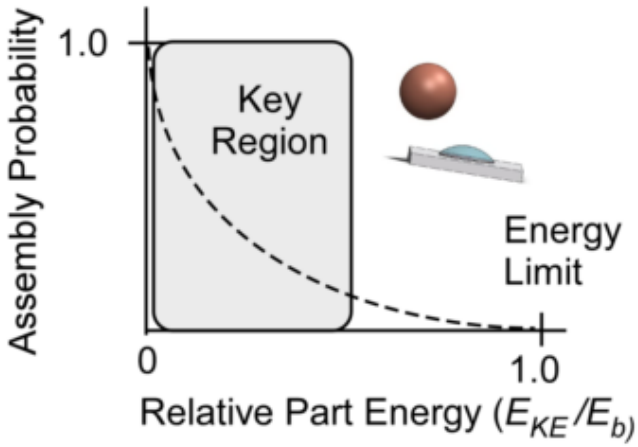

Figure 4-7: A spherical part's full surface is an assembly region. The geometric contribution to assembly probability due to the part to be 1.0

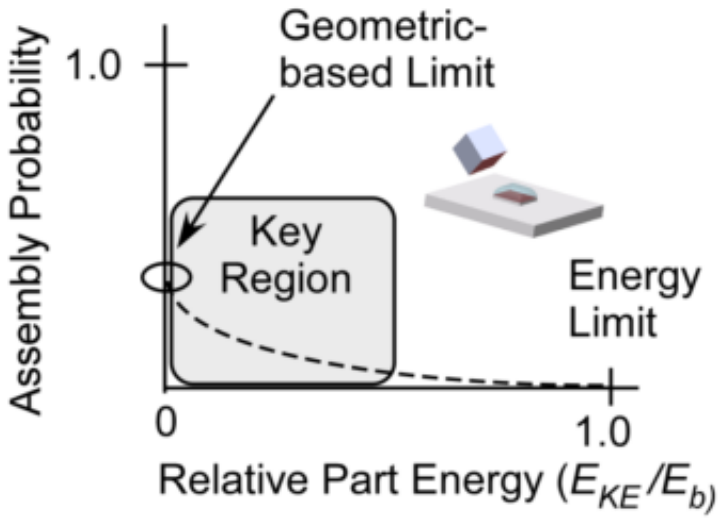

Figure 4-8: The geometric limit of assembly for a prismatic part. With only 1 active face this contribution to assembly probability is 1/6.

4.2.4 Assembly Component Fabrication

The assembly parts may be customized by appropriate selection of materials to affect the surface energy of the parts. Surface energy is affected through environmental fluid selection, material selection, and surface treatments. In the case of the techniques explored in the course of this research and the experimental setup SiO_2 wafers were coated with copper and treated with an n-octadecanethiol SAM to render copper coated regions hydrophobic. The SiO_2 wafers regions are not coated with the SAM as the active thiol head of the SAM is not adsorbed by silicon dioxide and so a difference in surface energy exists between the SAM coated copper regions and non-coated SiO_2 regions.

These surface characteristics determine the interaction bond energy of a bound assembly.

The sites and parts were fabricated with silicon wafers. Initially, a themal oxide coating was grown on the wafers. Next, Shipley 1813 Resist was spun onto SiO2 wafers then developed to expose the areas designated to be active. Using E-beam deposition 200 angstroms of Chromium followed by 500 Angstroms of Copper were deposited. The parts were then rinsed in Acetone to complete the liftoff process. This same formula of deposition was used on bare wafers which were coated and then diced into individual prisms to serve as parts for assemblies.

The patterned binding sites, thickness of the substrate, and diced size can be varied to achieve a variety of part aspect ratios and bond sizes to explore the effects of different sample cases upon the overall assembly process. Due to the application of dicing process and the strength of adhesion of the deposited materials to the substrate feasible part sizes using these methods range from several millimeters to approximately 100 microns.

After dicing, the Copper surfaces of the sites and parts were rendered hydrophobic by treatment with a SAM solution. The site arrays and parts were rinsed with ethanol and submerged in a 1mM solution of 1-octadecanethiol in 99% ethanol within a reduced Oxygen

environment for 24 hours along with Cu samples used to measure contact angles after treatment. Contact angles on SAM coated parts were measured using a contact angle goniometer. Results for contact angle measurements are shown in Table 4-1.

Table 4-1: Contact angles for copper treated with 1mM-Octadecanethiol SAM at various interfaces.

Fluid	Advancing Contact Angle
De-ionized water in air	114°
60% w/w glycerol/ 40% water in air	117°
n-hexadecane in air	16°

4.2.5 Bond Energy

The bond energy of the assembly sites is an important process parameter. The section above describing the application of Young's equation to the use of bond energy is important to understanding the effects of design choices on the system. The surface treatments applied to the sites effect the wettability of fluids on the sites. The copper sections of the assembly sites are treated with the 1-octadecanethiol SAM and are rendered further hydrophobic.

By applying an oil lubricant to the hydrophobic sites, a lubricating effect on the assembly can be observed, resulting in parts aligned more completely with the energy minima of the designed assembly site/part combinations. This oil is applied to the sites by passing the sites through a very thin layer of oil at the surface of the environmental fluid.

The hydrocarbon phase is composed of 0.4 mL of n-hexadecane. It is sufficient to treat several 2-inch strips of sites before requiring that it be recharged. This volume of fluid is contained within a glass passageway at the surface of the environmental fluid. The working passageway is cylindrical and 2cm in diameter. By passing the sites through the hydrocarbon phase and into the environmental fluid, which in the case of these experiments is either water or a solution of water and glycerol, the sites may be collected in a transport vessel submerged within the environmental fluid and then transported into a working vessel without removal from the environmental fluid.

The applied oil will bead over the sites initially, however agitation of the oiled sites with a fluid stream from a pipette will reduce the volume of fluid through shear and cause the sites to become more uniformly oiled.

Figure 4-9: Goniometer image of a droplet of oil applied to a site.

4.2.5.1 Verification of Oil Deposition

When the oil is deposited on the sites initially, it is possible for some bridging between sites to occur. This effect can be seen in the following image.

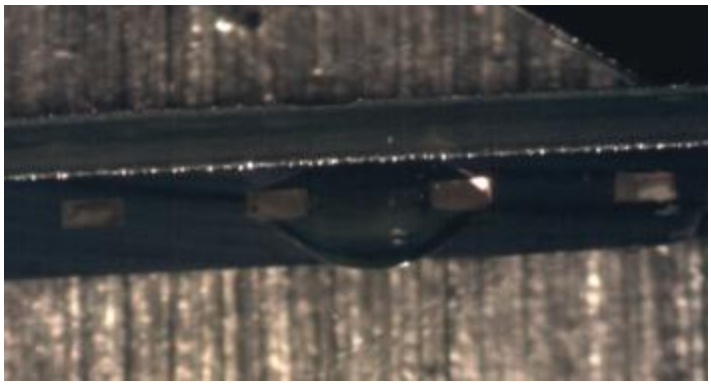

Figure 4-10: Assembly site strip with oil bridging assembly sites.

A strip of assembly sites treated with oil and agitated with the fluid flow from a pipette will create a regular array of oiled sites. The effects of this washing can be seen in the image below.

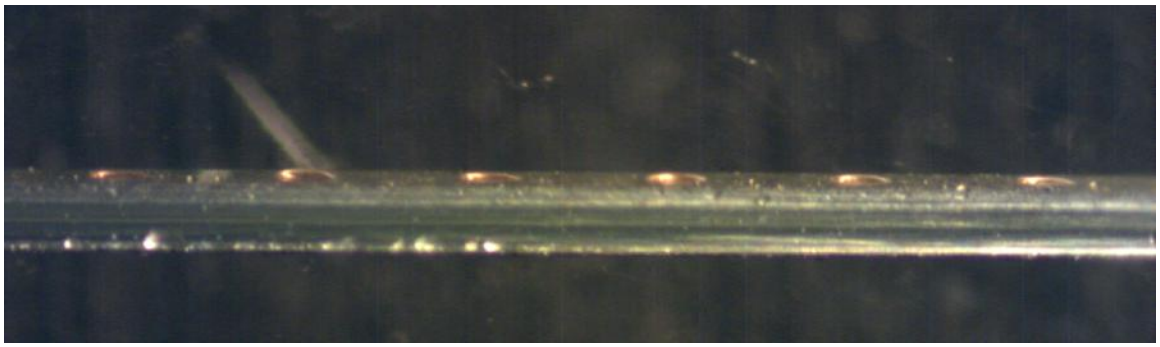

Figure 4-11: Oiled sites.

Measurements of the effects of pipette rinsing on the distribution of contact angles for oiled sites were made. These measurements indicate that the uniformity of the oil coating on these sites is improved. Measurements site strips containing a total of 29 sites were made and histograms generated for pre-rinsing and post-rinsing were made. The Averages and Standard deviations of the contact angles measured in these tests were calculated. These results are indicated in the following table.

Table 4-2: Site contact angles by treatment.

	Pre-Rinsed Sites	Post Rinsed Sites
Average Contact Angle	42.1	23.3
Standard Deviation	26.8	15.3

The table above indicates that the contact mean contact angle and deviation of the site's contact angle is effectively reduced through pipette washing. This is illustrated graphically in the following histograms.

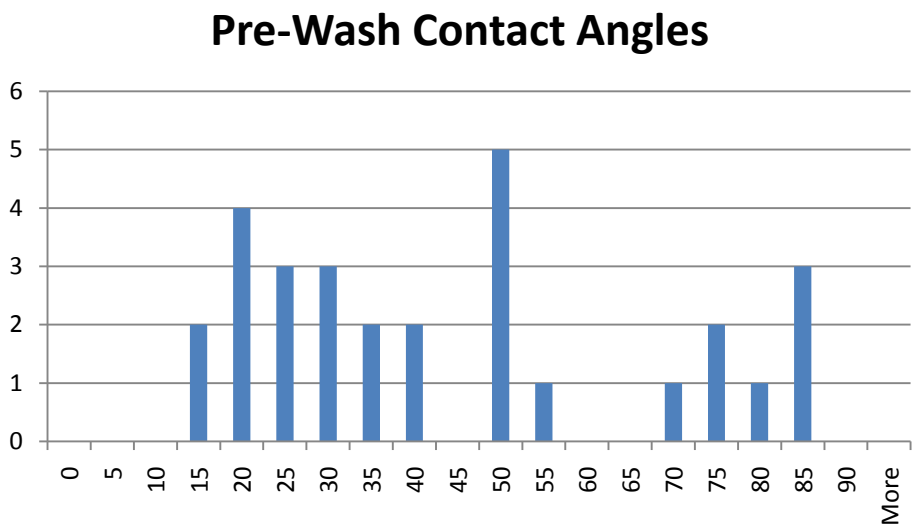

Figure 4-12: Contact angles for sites before washing with pipette. Sites were dip coated through hydrocarbon phase into aqueous solution.

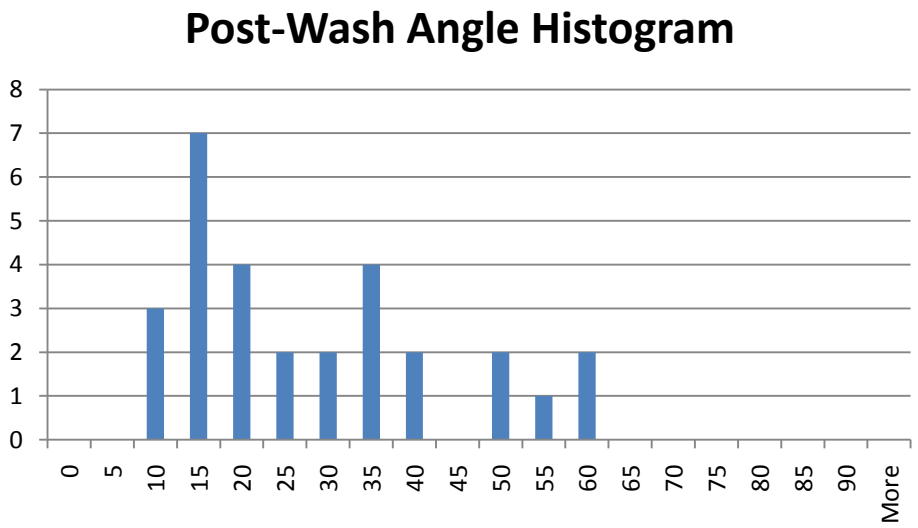

Figure 4-13: Contact angles for assembly sites after washing. The sites were dip coated through hydrocarbon layer into aqueous solution and washing with pipette flow of aquous solution.

This technique would improve greatly through the application of a pump to control the flow rate and volume of the fluid over the coated

sites. A peristaltic pump should be applied to this procedure in order to avoid contamination of the fluid within the pump. The current state of the technique is sufficient to ensure that individual sites are coated with oil while the regions outside of the copper assembly sites are free of oil. Without this washing, some bridging of oil from site to site is observed. The removal of oil from the inter-site regions is necessary to apply the current methods to test for the geometric assumptions of the model in which the area fraction of active assembly area is an important process characteristic. The bridge of oil, being hydrophobic, contributes additional assembly area to the overall assembly process.

The trials presented in the results section include trials conducted without the application of oil to the assembly surfaces. The assembly sites used in those tests are solid copper surfaces with no patterning. As lubrication of the assembly for proper site alignment has little meaning without patterned assembly sites, the oil patterning technique is not applied to these systems. However, the technique described above is important for future research.

4.2.6 Kinetic Energy Design

The kinetic energy of the interaction is controlled by the velocity of parts approaching assembly sites. This parameter can be controlled by designing the assembly environment to limit the part velocities to

the terminal velocity of the particles. The viscosity of the environmental fluid within the assembly structure can be used to set this limit because of the relationship between terminal velocity and kinetic energy. The parts will reach terminal velocity if the parts fall from sufficient height.

Fluid viscosity for the assembly environment can be varied by controlling the composition of the fluid as well as the temperature of the environment. This control is exercised over a continuum. In the assembly environment used for the purposes of this research, this is accomplished by varying the percentage of a glycerol to water in the environmental fluid mixture at room temperature. A significant change in viscosity can be achieved with only a modest change in surface energy (~10 mN/m) due to the variation in the relative interfacial energy between the capillary fluid and different compositions of environmental fluid. Interaction kinetic energy is also adjusted through manipulation of the solution and composition of the parts.

The range of kinetic energies achievable through this approach can be examined through calculations with spherical parts. The terminal velocity of spherical parts falling through a viscous medium is given by Equation 4-2.

$$V_t = \frac{gd^2}{18\mu}(\rho_f - \rho_s) \qquad \text{Equation 4-2}$$

In Equation 4-2, *g* is the acceleration due to gravity, *ρ* is the density of the fluid ρs, and μ is the dynamic viscosity of the fluid. In order to illustrate a range of terminal velocity values, Figure4-14 shows values for spheres of several diameters passing through a glycerol/water solution of varied concentration. These spherical terminal velocities are slightly higher than those found for flat plates at the same size and are useful, simple calculations for a limiting case.

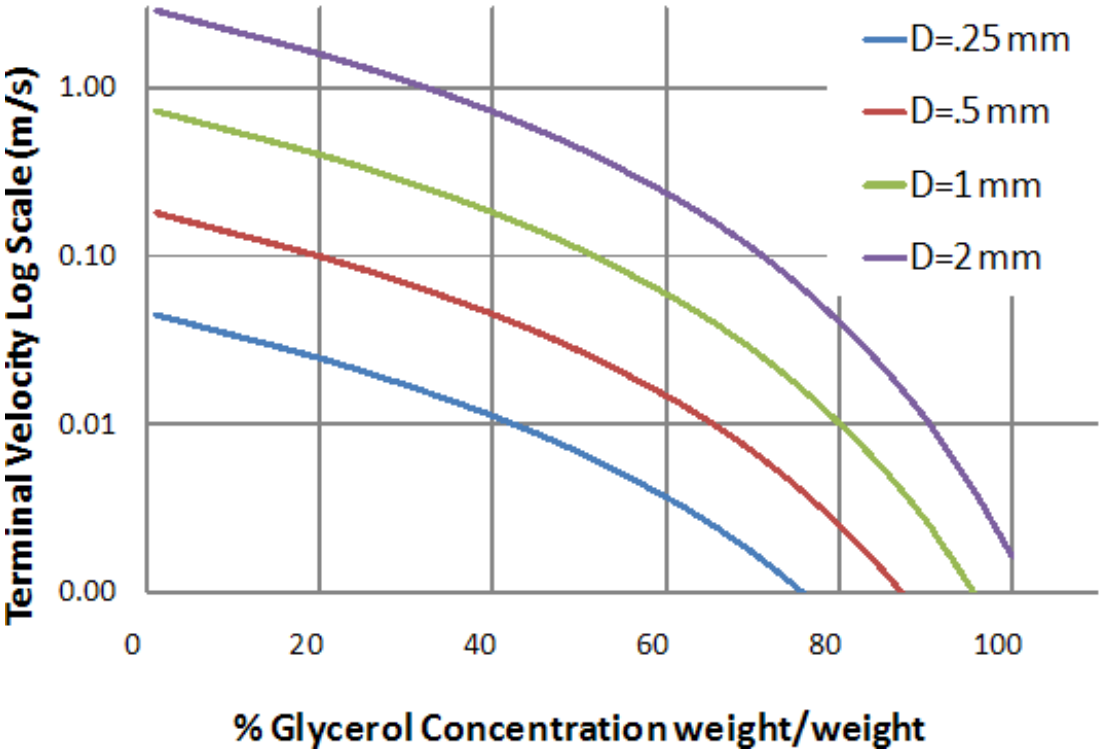

Figure 4-14 : Variations in terminal velocity. These variations may be achieved through particle size, density and fluid viscosity variations. These diameters range from .25 mm to 2 mm. The parts are composed of Silicon.

The component size, density, and shape all contribute to the terminal velocity of the components. The estimations of terminal velocity found through calculation of the spherical case provide limiting cases for design. However, these calculations should be compared to empirical measurement of the terminal velocity of the components falling through the fluid. A stroboscope was employed in order to conduct these measurements. Sample parts were introduced into a fluid column of the assembly environment's glycerol-water fluid at 60:40 weight to weight proportions, the same composition used within the assembly environment. The figure below shows a trial image for a prismatic part of with dimensions of 1mm X 1mm X .55mm composed of an SiO_2 wafer coated on two sides with Chromium and Copper as described in the assembly part fabrication section above. A camera was mounted on a tripod and exposed for one second while a strobe light flashed at 600 RPM within the field of focus. The falling parts reflected light back to the camera and calculations of the terminal velocity of the particles were made. The room was darkened during testing to improve the image contrast.

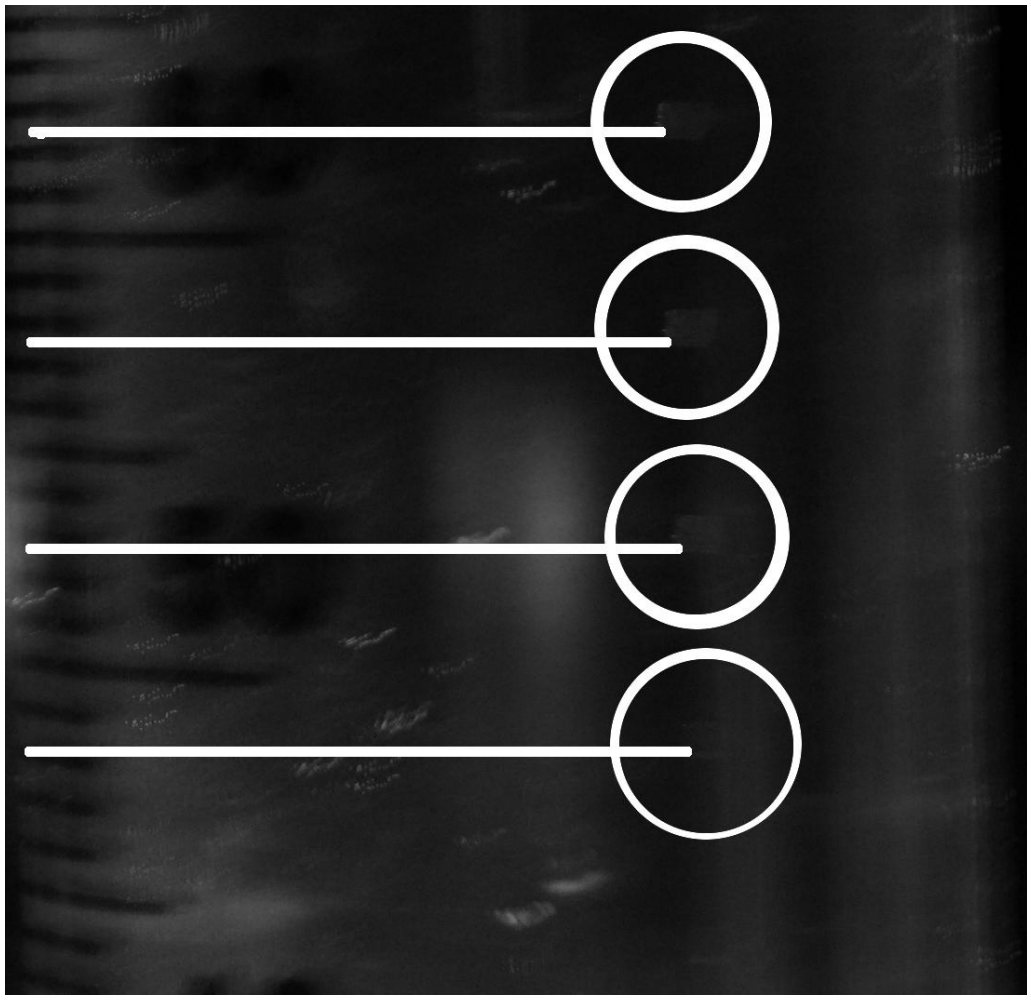

Figure 4-15: Stroboscope image of falling parts in fluid. White circles indicate the location of the part at a frequency of 600 Hz.

The measured terminal velocity for the displayed trial displayed in Figure 4-15 was 6.60 cm/s measured with a strobe at 600 RPM, which provided the clearest pictures of the strobe rates attempted. The spherical parts were calculated to have a terminal velocity of 14.1 cm/s. The Lack of uniformities in the parts will result in error in the approximation of the terminal velocity extrapolated from measurements of individual parts.

A second method for the measurement of velocity of falling parts was developed in order to help improve the quality of analysis. These tests were conducted with a set of parts smaller than those used previously, having the dimensions 0.5X0.5X0.55 mm diameter and composed of silicon with one face coated in copper. The fabrication of these parts is discussed in the following section. These parts were dropped through a fluid as a function generator triggered an Edward's Optics EO 2013C CMOS camera to capture images. The hardware signal provided an echo to a computer on which the system clock was correlated with the image capture to calculate the part velocity as the slope between the fall distance and time to fall. Multiple sequential images were analyzed for part location and timing and the velocity of the falling parts compared. The terminal velocity of the subject parts falling through a 40% glycerol to H_2O w/w solution was found to be 2.82 cm/s. The parts falling through de-ionized water fell with a velocity of 7.13 cm/s.

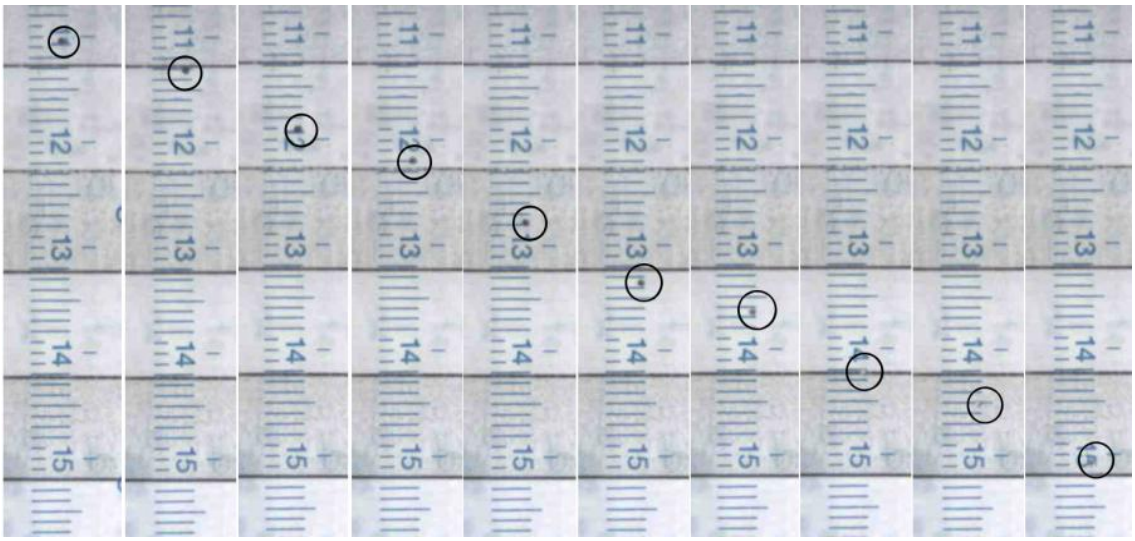

Figure 4-16: Falling part velocity images.

These trials were conducted five times for a 40% glycerol to H_2O solution at 25.7° C and five times for parts falling through water. The results are reported in Table 4-3. It can be seen there that the variation in velocities is relatively small between trials.

Table 4-3: Velocity measurement from 500μm sided parts through H_2O and 40% glycerol solution.

Fluid	Velocity Average	Velocity Standard Deviation
H_20 at 21.4 C	0.0725 m/s	0.0021 m/s
Glycerol at 21.0 C	0.0277 m/s	0.0005 m/s

Furthermore Figure 4-17 shows a linear regression for a plot of the distance fallen to the measured time. The coefficient of determination 0f 0.9902 shows a good fit to the linear regression indicating that the points fall very closely to a line. The linear fit of the distance to time measurements indicates that the parts are falling at terminal velocity and not accelerating through the fluid.

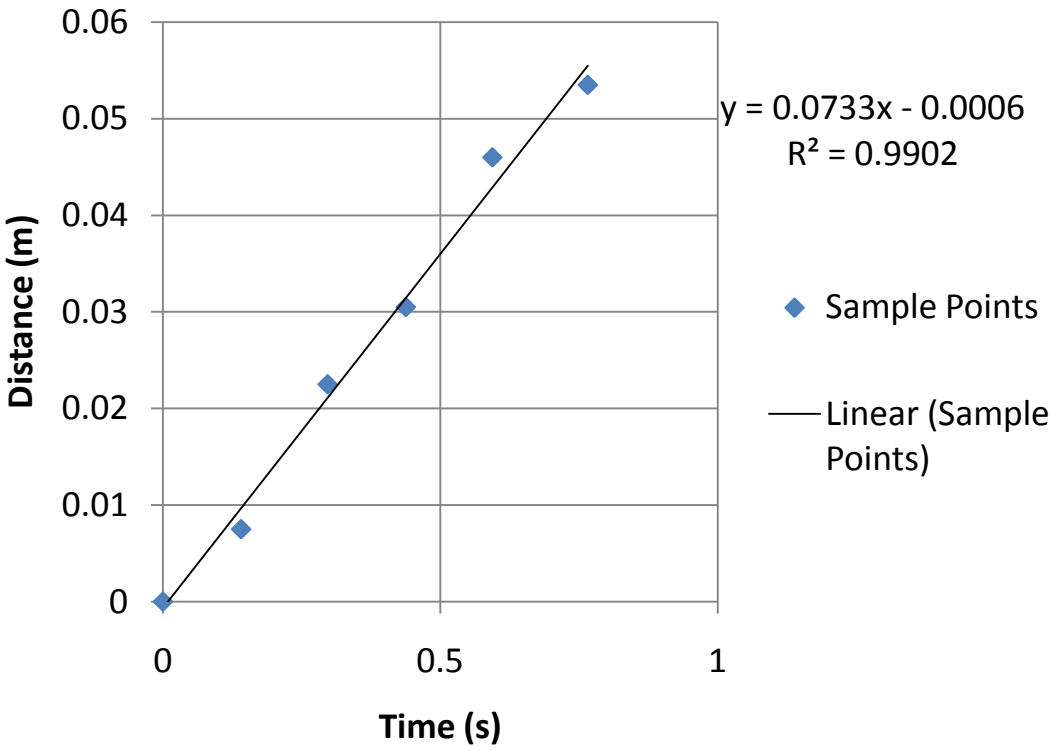

Figure 4-17: Linear regression from time trial.

The velocity of the parts is related to the kinetic energy of the interaction through the relationship shown in Equation 4-3.

$$E_{KE} = \frac{1}{2}mv^2 \qquad \text{Equation 4-3}$$

Relative variations in the velocity will have the greatest effect on the kinetic energy of the parts due to the square proportionality between kinetic energy and velocity. In studying the effects of the kinetic energy to bond energy ratio described in the next section of this thesis it is important to ensure that these variations do not interfere with the resultant picture of the relationship. In order to do so, the researchers conducted experiments wherein the parts were

structured and the viscosity of the fluid was selected so that the terminal velocity of the parts was well below or above the kinetic energy to bond energy ratio of 1:1.

4.2.7 Energy Ratio: Kinetic Energy to Bond Energy

The ratio of kinetic energy to bond energy for an assembly interaction may be an important process parameter. With many parallel assembly processes occurring without feedback based control systems it is important to ensure that the parts engage in the binding process with a lower kinetic energy than the energy minimized through binding. In this way, the bonds may be formed without immediate release from the bond. Furthermore, additional interactions between free floating parts and bound parts will not result in assembled parts being dislodged from their position. Through the control of assembly velocity and capillary bond energy, the ratio of these two parameters can be ensured. The kinetic energy of the assembly interaction between a falling particle and a fixed substrate can be varied with the terminal velocity as illustrated above.

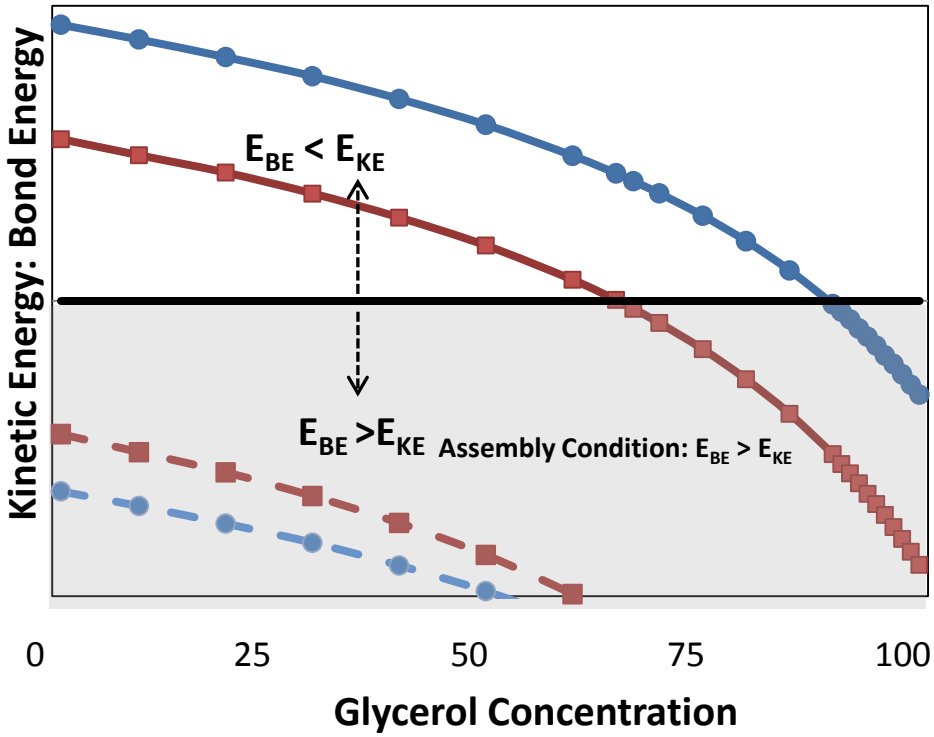

Figure 4-18: Assembly condition in the grey region. This region is below the 1:1 Kinetic to Bond Energy Ratio.

Figure 4-18 graphically demonstrates the region in which assembly conditions are favorable while disassembly conditions are unfavorable. Curves indicate the energy ratio for arrangements of process characteristics for the assembly of cubic parts over a range of glycerol concentrations within the proposed assembly environment. The lines marked with squares indicate assemblies using n-hexadecane as the assembly binding fluid with a surface energy density of 0.025 J/m^2. The lines marked with circles indicate assemblies with a higher energy density fluid, a low melting point solder with a surface energy density of 0.5 J/m^2. The dashed lines indicate smaller parts with 0.25

mm squares while the large parts indicate parts with 2mm square profile areas. The large parts, solid lines, can exceed the KE:BE energy ratio at Unity for The majority of glycerol concentrations for either binding fluid. However, there are regions in which even these large parts can be used in assembly. For either composition of fluid and part size there exists a wide range of process parameters which may be selected to favorably affect bond stability, however it is important to apply an appropriate analysis before attempting assembly.

The bond energy for a thin film of capillary fluid between components of equal size can be approximated as the bond for the case of a small amount of fluid as shown in Equation 4-4. This relationship between surface energy density γ and the profile area of the bonded between the components is important to the design of the assembly parts and assembly sites. The composition of the liquid/assembly medium and solid/assembly medium determines the interfacial surface energies for the bond while A is the bond area

$$E_B = (\gamma_{lm} - \gamma_{sm})A_b \qquad \text{Equation 4-4}$$

CHAPTER 5: EXPERIMENTATION AND RESULTS

Several trials of self-assembly processes have been conducted with the previously described assembly environment. These trials have been, in large part, conducted with the intention of refining new techniques for application within the micro-scale integration lab. The results do however reveal some relationships which may be explored in greater detail in further studies conducting using the methods under development here.

The researchers hypothesize that the assembly yield may be predicted through appropriate application of a Markov chain model of self-assembly. Several process variables are under investigation. The geometric contribution to assembly should dictate the assembly yield when the kinetic energy to bond energy ratio is near zero. Furthermore, because the assembly bond action is driven by surface energy, the bond energy parameter may be applied with the assumption of path independence and part approach angle will not affect the assembly, though projected area of assembly due to angular variations in the site mounting will make a contribution to the assembly yield.

Five trials are reported upon. These were conducted using the self-assembly test system developed for research into self-assembly modeling. The tests were conducted with the intention of evaluating the state of processes available currently and to identify process weaknesses, model applicability at the current time, and further direction in the application of these processes to self-assembly research.

These trials were conducted using parts described in Chapter 4 of this thesis. The faces of these parts are shown in the image below.

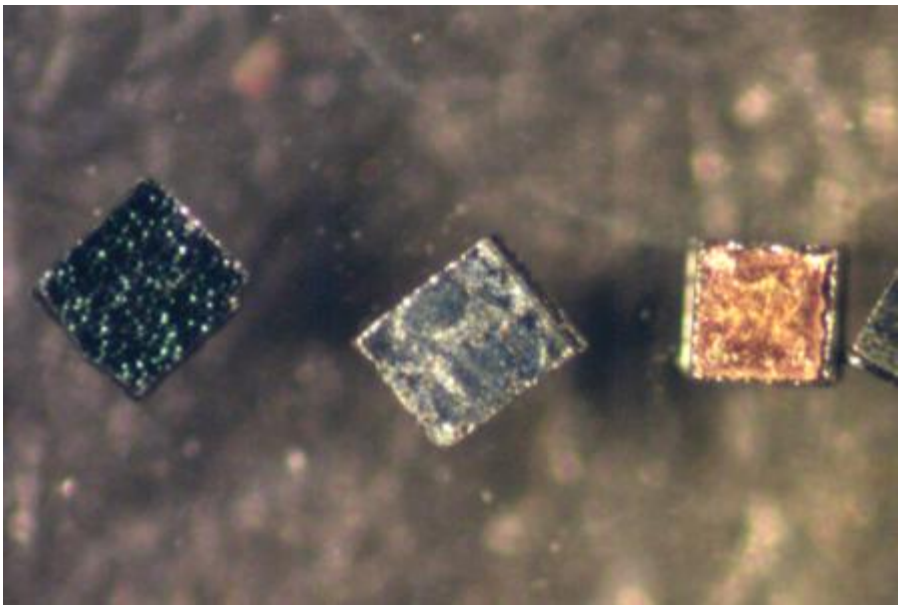

Figure 5-1: Fabricated parts. From left to right: The SiO_2 face of an assembly part, the diced edge of an assembly part, and the Copper coated face of a part

The parts, in all trials, were diced and coated with a 1-octadecanethiol solution as discussed previously in Chapter 4 under "Assembly Component Fabrication." This treatment renders the copper

face of the sites hydrophobic, while the SiO_2 face of the part remains hydrophilic. The part and site pairings for each trial are summarized in Table 5-1. The notation for the bonding fluid, C8 SAM, refers to the SAM n-octadecanethiol.

Table 5-1: Assembly trial details.

Trial	Part Dimensions	Site Structure	Fluid Environment	Bonding Fluid
A-1	1 X 1 X 0.55 mm^3	Patterned Cu 1 X1 mm2 sites on SiO_2	60% Glycerol: H_2O	hexadecane
B-1	0.5 X0.5 X0.55 mm^3	Cu Faced strips	40% Glycerol: H_2O	C8 SAM
B-2	0.5 X0.5 X0.55 mm^3	Cu Faced strips	H_2O	C8 SAM
B-3	0.5 X0.5 X0.55 mm^3	Cu Faced strips	H_2O	C8 SAM
B-4	0.5 X0.5 X0.55 mm^3	Cu Faced strips	H_2O	C8 SAM

The pattered Cu assembly sites for trial A-1 are discussed in detail in chapter 4. The Cu Faced strip assembly sites for the B series of assembly tests can be seen in Figure 5-2. These sites are 1.88 mm wide strips of silicon wafers with Copper deposited on SiO_2 as described in Chapter 4 under "Assembly Component Fabrication". These depositions were made onto the entire face of SiO_2 wafers without patterning the surface through the photolithography and liftoff process used to create the patterned Cu assembly sites used in trial A-1. In all trials the sites were treated with the same 1mM 1-octadecanethiol SAM solution used for the parts rendering the copper face hydrophobic. These sites were then mounted within the assembly

fixture, placed in the assembly environment, and the environmental fluid for the trial was added.

The introduction of fluid to the environment, in the current process, may introduce bubbles to the environment. These bubbles can be seen in Figure 5-2.

Figure 5-2: Assembly sites with bubbles.

In order to prevent these bubbles from interfering with the assembly a vacuum is pulled on the fluidic environment to remove gas from the fluid. Any remaining bubbles are washed free with a pipette. The resulting surfaces are clear of contamination and bubbles which would otherwise interfere with the uniformity of surface properties within the assembly environment.

Figure 5-3: Assembly array after purging of bubbles.

The preceding steps were repeated for each trial. The trials A-1 and B-1 conducted included the application of the assembly process to site strips mounted at 45 degrees within a glycerol solution to control the falling parts' terminal velocities. The remaining trials were conducted with deionized water as the environmental fluid and with sites mounted at 45 degrees in trial A-2, 60 degrees in Trial A-3, and 30 degrees in Trial A-4. These angles are relative to the incoming part trajectories and used with the intention of observing the effects of

change in projected area to the stream of incoming parts upon the final yield of the system.

5.1 Experimental Parameters

The following sections present the geometric and energetic parameters for the experimental trials conducted using the self-assembly test system.

5.1.1 Energetic Relationships

The assumption of a near zero energy ratio of kinetic energy to bond energy must be verified discussed in the section on modeling allows for the yield predictions to be made at the geometric limit of assembly.

5.1.1.1 Kinetic Energy in Trials

In order to use this assumption, the velocimeter measurements described in section *4.2.6 Kinetic Energy Design* were used to calculate the kinetic energy for the parts. These were calculated and are tabulated below in Table 5-2.

Table 5-2: Kinetic energy for trials.

Trial	Fluid	Part dimensions	Part mass (kg)	Velocity (m/s)	Kinetic Energy (J)
A-1	60% glycerol:H_2O	1X1X0.55 mm^3	1.0E-6	5.01E-2	1.26E-9
B-1	40% glycerol:H_2O	0.5X0.5X0.55 mm^3	2.5E-7	2.77E-2	9.65E-11
B-2	H_2O	0.5X0.5X0.55 mm^3	2.5E-7	7.25E-2	6.58E-10
B-3	H_2O	0.5X0.5X0.55 mm^3	2.5E-7	7.25E-2	6.58E-10
B-4	H_2O	0.5X0.5X0.55 mm^3	2.5E-7	7.25E-2	6.58E-10

5.1.1.2 Bond Energy in Trials

To find the Energy ratio for these trials it is necessary to calculate the bond energy for each trial. The bond energy calculations are described under section *4.2.5 Bond Energy*. The results of the bond calculations and the parameters associated with the calculation of bond energy are tabulated below. These calculations were carried out with the assumption that the n-hexadecane bonding fluid was of sufficiently small volume that its surface area could be assumed to be equal to the area that it wets. The notation for the bond fluid C8 SAM refers to n-octadecanethiol self-assembled monolayer. The total bonded area is the area of the site area of a single active part face and the area that that part face makes contact with in the assembly.

Table 5-3: Bond energy and associated parameters for assembly trials.

Trial	Environmental Fluid	Bond Fluid	Bonded area (m^2)	Bond Energy (J)
A-1	60% glycerol:H_2O	n-hexadecane	2.00E-6	2.10E-8
B-1	40% glycerol:H_2O	C8 SAM	5.00E-7	2.79E-8
B-2	H_2O	C8 SAM	5.00E-7	2.79E-8
B-3	H_2O	C8 SAM	5.00E-7	2.79E-8
B-4	H_2O	C8 SAM	5.00E-7	2.79E-8

5.1.1.3 Energy Ratio in Trials

The energy ratio for the trials must be calculated in order to determine if the zero energy ratio assumption can be held. The results of these calculations are shown in Table 5-4. The energy ratios found through these calculations are well below 1:1 and so, if the assumption of a near zero energy ratio is valid then the yield for these assemblies should be predictable based upon the geometric limitations to assembly.

Table 5-4: Energy ratio for assembly trials.

Trial	Kinetic Energy (J)	Bond Energy (J)	Energy Ratio
A-1	1.26E-9	2.10E-8	0.059
B-1	9.65E-11	2.79E-8	0.003
B-2	6.58E-10	2.79E-8	0.023
B-3	6.58E-10	2.79E-8	0.023
B-4	6.58E-10	2.79E-8	0.023

5.1.2 Geometric Relationships

The assembly interaction includes a collision between introduced parts and stationary assembly sites. In order for an assembly to occur, the hydrophobic faces of the parts must come into contact with the hydrophobic region of the assembly sites whether they be patterned sites as in trial A-1 full faced assembly strips as in the B series of trials. When this interaction does occur, capillary forces associated with surface energy minimization will attempt to bind the assembly part to the assembly site. However, if the kinetic energy of the interaction is too great these forces may be overcome as the parts

break free of the sites. Therefore, it is expected that there should be a peak assembly yield value at zero kinetic energy. At this limiting value, everything that contacts favorably will bond.

The area fraction of available binding area to the total assembly environment depends upon the orientation of the binding sites as well as to the geometry of the assembly mounts. The total assembly area represents the area over which the parts are uniformly distributed, i.e. the full assembly environment bounded by the acrylic walls of the assembly chamber. The area of interest within the assembly environment is the region in which assembly sites are mounted and between the mount edges. Parts are distributed outside of this area, however, this is the only area in which assemblies may take place.

For each assembly trial, the active fraction of the assembly environment in which assemblies may take place is proportional to the cosine of the orientation of the sites.

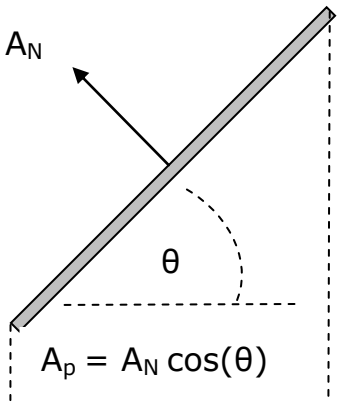

Figure 5-4: Projected assembly area as a function of mount angle.

For the assembly trial A-1 assembly sites were composed of 1mm^2 regions. The trials were conducted in an early version of the assembly environment with the following geometric characteristics.

Table 5-5: Trial A-1 assembly geometry.

Assembly Area Geometry Trial A-1	
Total Area of Uniform Part Distribution	2823 mm^2
Total Mounted Strips	21
Sites per strip Average	14
Area Fraction of Cu 1mm^2 sites on patterned strips	0.0793
Area fraction of strip projected parallel to fluid surface	0.0740
Area Fraction of sites projected parallel to fluid surface	0.06
Geometric limit to assembly	0.03

For the assembly trial series B, there are a total of 25 assembly strips in each trial. The assembly site area is multiplied by the cosine of the tilt angle resulting in the projected area of the assembly sites.

$$A_f = \frac{A_s \times \cos(\theta)}{A_T} \qquad \text{Equation 5-1}$$

This area is divided by the total area of the environment to find the area fraction of active assemblies. The Area fraction is later multiplied by 1/6 as each part is a cube in which one of the six faces is a valid assembly location.

Table 5-6: Trial B series assembly geometry.

Assembly Area Geometry Trial Series B	Area Fraction	
Total Area of Assembly Environment	5642 mm^2	1
Area of Interest within environment	2157 mm^2	0.3823
Number of site strips in each trial	25	
Active Area of site strip	68.3 mm^2	
Total Active Area	1707.5 mm^2	0.3026
Trial B-1 Active Area at 45º	1207.1 mm^2	0.2139
Trial B-2 Active Area at 45º	1207.1 mm^2	0.2139
Trial B-3 Active Area at 60º	853.5 mm^2	0.1513
Trial B-4 Active Area at 30º	1478.5 mm^2	0.2621
1/6 active area for prismatic parts		0.16667
Trial B-1 Geometric limit to assembly		.036
Trial B-2 Geometric limit to assembly		.036
Trial B-3 Geometric limit to assembly		.025
Trial B-4 Geometric limit to assembly		.044

As described within the section on unit cell dynamics for the assembly interactions, the yield predictions for this model include the active area fraction of the surface of the assembly parts. The total yield prediction includes a function describing the effect of the KE:BE ratio. However, in the following experiments all trials are assumed to be conducted with a near zero energy ratio, kinetic energy:bond energy. With this assumption in place the predicted yields are at the geometric limit to assembly.

Table 5-7: Assembly yield predictions.

Assembly yield predictions for Trial sets A and B	
Trial A-1 Yield : 60% glycerol at 45^0 to normal	.03
Trial B-1 Yield : 40% glycerol at 45^0 to normal	0.0357
Trial B-2 Yield : Deionized H2O at 45^0 to normal	0.0357
Trial B-3 Yield : Deionized H2O at 60^0 to normal	0.0252
Trial B-4 Yield : Deionized H2O at 30^0 to normal	0.0437

5.2 Experimental Results

The trial results and predicted yield are tabulated below in Table 5-8: Trial results and yield predictions.

Table 5-8: Trial results and yield predictions.

Trial	Predicted Yield at Zero KE limit	Parts Dropped	Parts Bound	Resultant Yield
Trial A-1 Yield : 60% glycerol to H2O at 45^0 to normal	0.03	170	5	0.029
Trial B-1 Yield : 40% glycerol to H_2O at 45° to normal	0.0357	2664	107	0.0402
Trial B-2 Yield : Deionized H_2O at 45° to normal	0.0357	3126	33	0.0106
Trial B-3 Yield : Deionized H_2O at 60° to normal	0.0252	3268	11	0.0034
Trial B-4 Yield : Deionized H_2O at 30° to normal	0.0437	3282	189	0.0575

5.3 Comparison to Hypotheses

The results of the trials show mixed results in comparison to the experiment hypothesis. Trial A-1 shows the closest yield to the predicted yield. This trial included fewer parts dropped onto a patterned substrate. The predicted yield is shown as a function of substrate mount angle. The hypothesis for these trials is that for systems in which the kinetic energy of the assembly interaction is low in comparison to the bond energy of an assembly the predicted yield will be at the geometric limit to assembly. With the self-assembly test system all parameters of the assembly are fixed for a given trial,

however, within a trial series the substrate mount angle may be changed or fluid altered. In the case of trial A-1 the first prototype of the test system was in use and so the geometric limit of assembly, i.e. the predicted assembly yield, is different than the B series of trials. Trial A-1's curve and results are shown in Figure 5-5. The curve and results for Trial series B are shown in Figure 5-6.

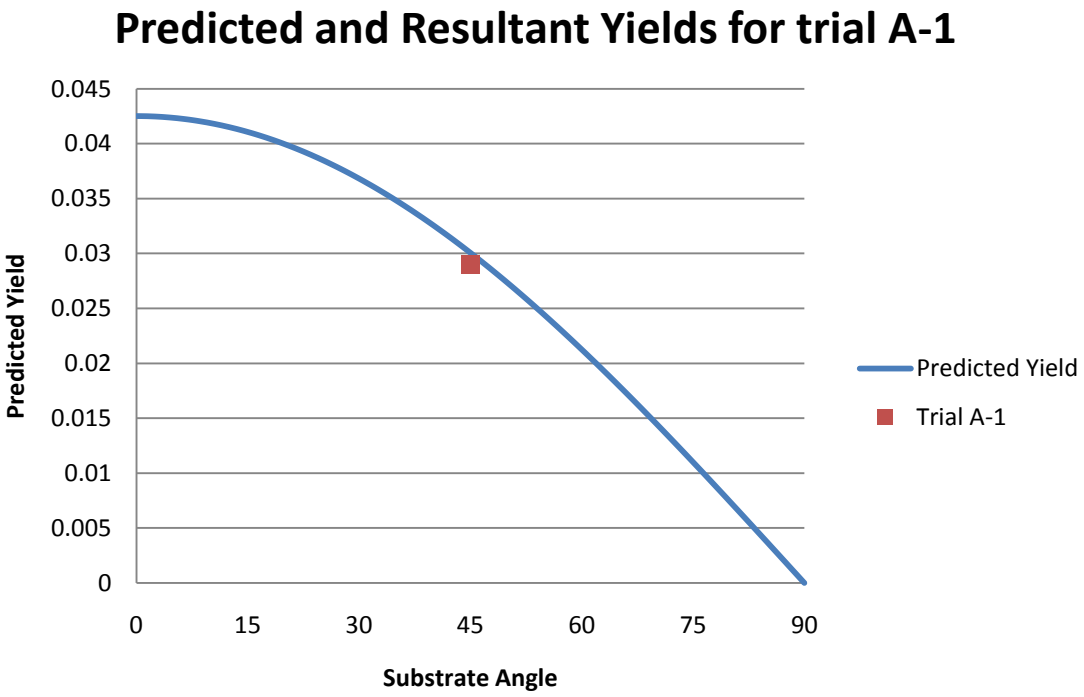

Figure 5-5: Predicted yield curve with trial A-1 data point. The predicted yield is a function of the substrate angle as the tilt of the substrate will alter the area of active assembly projected normal to the travel of parts.

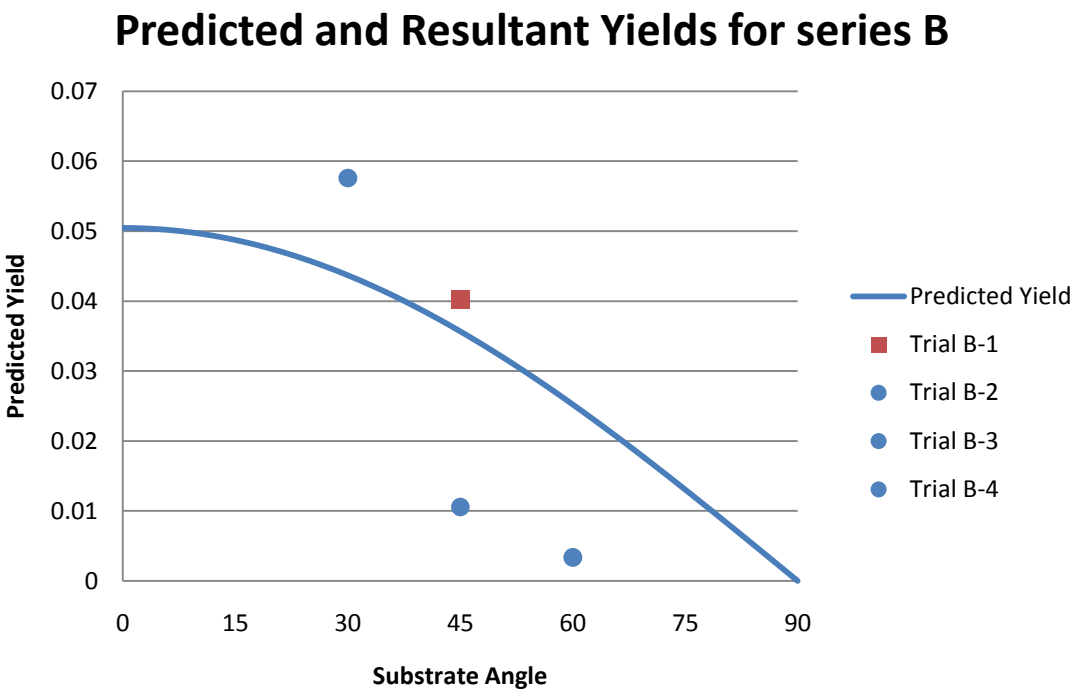

Figure 5-6: Predicted and resultant yields for trials. Trial B-1 was conducted in 40% glycerol to H_2O and is depicted using a square data point marker. The remaining tests were conducted in de-ionized H2O and are depicted with circular data point markers. The substrate angle affects the geometric limit of assembly.

5.3.1 Trial A-1

This trial was conducted in an 60% glycerol to de-ionized water environment with sites oriented at 45° to the direction of travel of the sites. 170 parts were dropped over the assembly environment and 5 successfully bound to the patterned assembly sites. The yield in this case was 0.029 of the total dropped parts. This trial was conducted near the zero energy limit wherein the geometric parameters dominated the assembly model. This outcome is in good agreement with the predicted 3% yield. Unlike the other trials, this trial was

conducted with few parts. This may account for the high accuracy of the predicted yield as the number of part interactions interfering with the assembly would be reduced.

5.3.2 Trial B-1

The first trial of this series, conducted in an 40% glycerol to de-ionized water environment with sites oriented at 45º to the direction of travel of the sites. 2664 parts were dropped over the assembly environment and 107 remained attached to the assembly area. The yield in this case was 0.04016 of the total dropped parts. This trial was conducted near the zero energy limit at which the geometric parameters of the assembly model dominate yield.

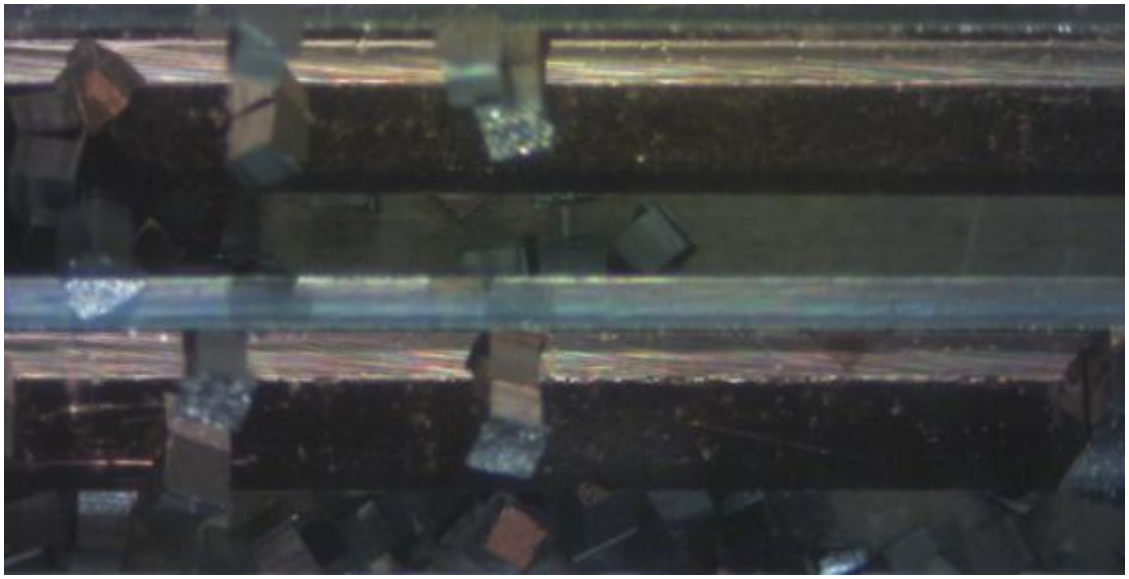

Figure 5-7: Parts shown adhering to the copper site strips. The strip on top shows two parts bunching together from the continued addition of parts to an occupied area.

The yield in this trial is somewhat higher than the predicted value of 0.0357. The grouping of parts at successful assemblies may be the cause. Parts landing on the surface, but in the wrong orientation, could simply remain in place due to contact with a properly attached part. The current setup is insufficient to test this speculation however, as it is unclear if the parts gathered as they fell or after falling to the surface.

5.3.3 Trial B-2

The second trial was conducted in de-ionized water with assembly strips oriented at 45º to the direction of part travel. 3126 parts were introduced to this environment with 33 parts assembling to the face of the copper in a recognizable fashion. A total of 88 parts remained on the surface, however most of these formed accretions which are difficult to analyze and point to a necessity for some modification to part design or assembly process to prevent these formations from developing.

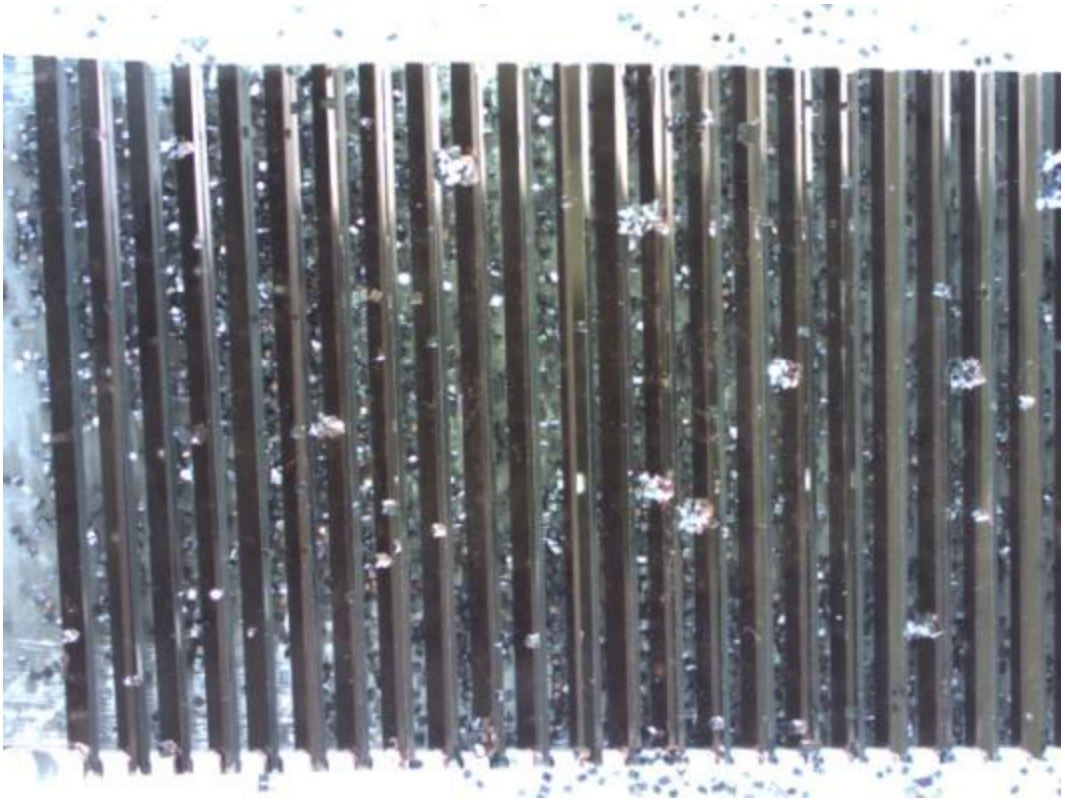

Figure 5-8: Trial B-2 assembly results.

The yield of Trial 2 is found to be 0.0106, well below the predicted yield of 0.0357. This result is in part due to the difficulty of accounting for the accretions of parts, and also due to the anticipated effect of the higher energy interactions encountered in a pure H_2O environment in which the kinetic energy of the parts exceed the bond energy of the parts.

5.3.4 Trial B-3

The third trial was conducted in de-ionized water with assembly strips oriented at 60º to the direction of part travel. 3268 parts were

introduced to this environment with 11 parts assembling to the face of the copper in a recognizable fashion. A total of 46 parts remained on the surface, however many of these formed accretions which are difficult to analyze as discussed previously.

Figure 5-9: Trial B-3 assembly. The sites are oriented at 60 degrees to the direction of travel of parts

The yield of Trial 3 is found to be 0.00336, well below the predicted yield of 0.02521. This result is in part due to the difficulty of accounting for the accretions of parts, though, even accounting for all accreted parts as successful bonds the yield would remain low. The anticipated effect of the higher energy interactions encountered in a

pure H_2O environment in which the kinetic energy of the parts is an additional factor which would interfere with the clarity of these results.

A successfully bonded part is shown below as well as an image of the accretions encountered in all of the assembly trials.

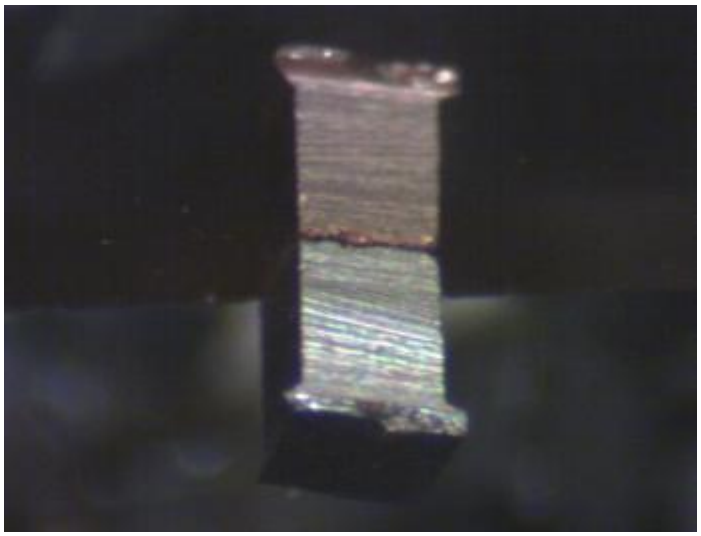

Figure 5-10: Successfully bound part in assembly trial B-3. Note that this part suffers from a fabrication flaw due to dicing error. The parts reflection on the substrate makes ita appear like two parts.

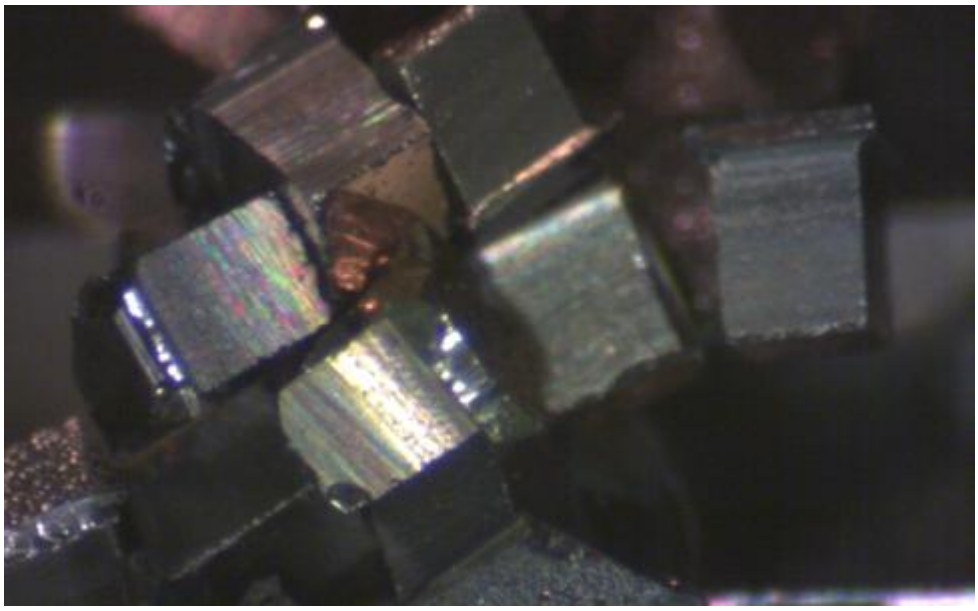

Figure 5-11: An accretion of parts observed in assembly trial B-3.

5.3.5 Trial B-4

The fourth trial was conducted in de-ionized water with assembly strips oriented at 30º to the direction of part travel. 3282 parts were introduced to this environment with 189 parts assembling to the face of the copper in a recognizable fashion. The yield of this trial was 0.05758, exceeding the predicted yield of 0.04368.

Figure 5-12: Results of trial B-4.

The high yield in this trial indicates that a simple geometric model for the interaction may be insufficient to describe the dynamics of the assembly interactions. With the sites at 30° to the direction of travel of the parts, the parts are likely encountering the sites and coming to rest on the sites whether they bind or not due to the low contribution of gravity to the motion of the parts in contact with the copper sites. The following picture shows several parts resting on the assembly sites without their copper faces binding to the strips as a result of the failure to move beyond the binding region.

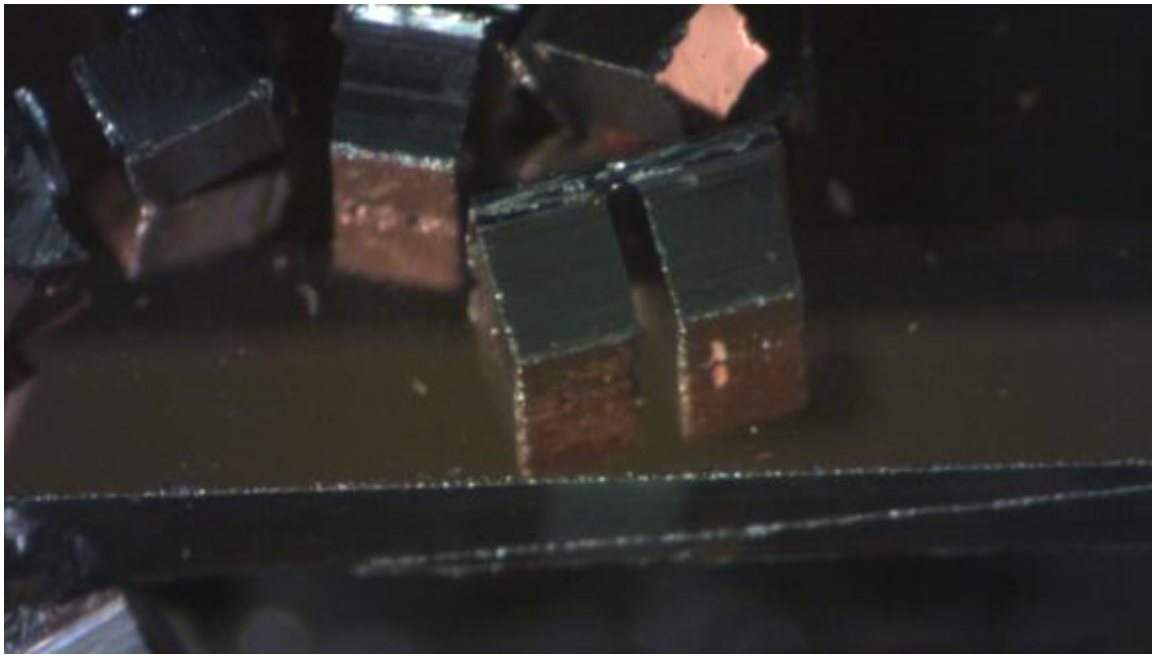

Figure 5-13: Parts resting on assembly sites. These parts remain in place without binding to them properly and without accreting to one another in trial B-4.

Because the parts which strike the area of interest, but in the wrong orientation are capable of resting on the site, then the potential area of interest assembly is six times the assembly for parts striking in the correct orientation. The higher pitched substrates used in the other trials may permit the parts to slide off of their resting places if not successfully bound to the sites. In this trial, parts remain in place no matter their initial contact orientation or the result of a successful or unsuccessful binding.

The results of this trial emphasize the necessity for a repulsive force within the self-assembly environment. If the assembly had been conducted with a force of sufficient magnitude to repel parts from the

resting state in which they lie if unassembled, then the final yield count would be reduced to include only parts that approach the assembly in an orientation to bind to the site.

CHAPTER 6: CONCLUSIONS

The application of the test environment to the initial assembly trials has revealed some important test design parameters. These conclusions will be acknowledged in the design and implementation of future experimentation plans using the system presented here.

The high relative accuracy of the trial A-1 compared to the B series of trials indicates a need to design tests using fewer parts, or to modify the system to prevent part interactions. This follows with the background from chemical kinetics in which rate law models are created through the application of test data acquired during the first 10% of a reaction, as described in the background section of this work. Future trials will be conducted with fewer parts so that a sparse distribution assumption for non-interaction will be valid.

The lack of a repulsive force within the environment can result in difficulties modeling and evaluating the performance of an assembly. The chemical kinetics models do not account for near chemical reactions in the way that may be seen in micro-scale mechanical interactions between parts. The trial B-4 showed that parts may remain in the assembly space even without successfully binding if the repulsive force for disassembly of misaligned parts is too low to

remove them from the region. In this case, the repulsive force would be gravitational and the tilt of the assembly sites was insufficient to allow the gravitational parts to overcome the friction found resting on the assembly sites, even without a capillary bond in place.

Some promising results have been seen from the application of the Self-Assembly test system developed for the purposes of this research. The modeling, which still requiring a great deal of fleshing out, appears at an initial assessment to reflect the assembly performance when the appropriate assumptions are observed.

6.1 Future Work

In the short term it is the recommendation of this researcher that further trials be conducted exploring the near zero energy ratio limit assumption. A sequence of test conducted with varied fluid viscosity would greatly help to gather the sample data necessary to develop a proper functional model of the contribution of higher kinetic energies to the overall assembly yield.

Furthermore, test repetitions using controlled forces for free part rejection may improve the clarity of assembly yield results. The automation of such a system would be ideal as consistency and repeatability should be observed in these trials. A peristaltic pump

connected to the assembly environment would provide a consistent flow, however, pulsations in the flow may be desirable.

The interference of individual parts within the assembly trials may be reduced or eliminated by changing the spacing of assembly sites and the spatial distribution of part drops. The interference of parts is a difficulty which affects analysis adversely and should be addressed as soon as possible. In a high throughput industrialized processes it seems likely that part interference may be unavoidable. Modifying the predictive model to account for interference would, for this reason, be desirable.

Further characterization and evaluation of the part and site fabrication process could be fruitful. The researcher and his colleagues have observed flaws in the copper surfaces of the sites and parts, as well as residual copper left after the copper liftoff process has been completed for patterned assembly areas.

Surface energy for assembly bonds may be increased by employing a silane SAM treatment to the Si surfaces of the assembly components. A hydrophilic silane would reduce the surface energy for the Si portions of the assembly environment. Because the assembly surfaces are bounded by silicon regions the reduction in surface energy of the silicon regions would increase the gradient of energy between the assembly surfaces and the non-active assembly regions, improving

the bond strength and increasing the capillary forces at play during bonding.

LIST OF REFERENCES

[1] Pelesko, J. A., 2007, "Self assembly: the science of things that put themselves together," Taylor & Francis, Boca Raton.

[2] Morris, 2005, "Self-Assembly for Microscale and Nanoscale Packaging: Steps Toward Self-Packaging," IEEE Transactions on Advanced Packaging, 28(4) pg. 600.

[3] Hsi-Jen, Y., 1994, "Fluidic self-assembly of microstructures and its application to the integration of GaAs on Si," pg. 279.

[4] Yeh, H.- J., 1994, "Fluidic Self-Assembly for the Integration of GaAs Light-Emitting Diodes on Si Substrates," IEEE Photonics Technology Letters, 6(6) pg. 706.

[5] Verma, A. K., 1995, "Fluidic self-assembly of silicon microstructures," pg. 1263.

[6] Bohringer, K. F., 2001, "Modeling of Capillary Forces and Binding Sites for Fluidic Self-Assembly," pg. 369.

[7] Greiner, A., Lienemann, J., Korvink, J. G., 2002, "Capillary forces in micro-fluidic self-assembly," 2002 International Conference on Modeling and Simulation of Microsystems - MSM 2002, Apr 21-25 2002, Anonymous Computational Publications, Cambridge, MA 02139, United States, San Juan, Puerto Rico, pp. 198-201.

[8] Scott, K. L., 2004, "High-Performance Inductors using Capillary Based Fluidic Self-Assembly," Journal of Microelectromechanical Systems, 13(2) pg. 300.

[9] Srinivasan, U., 2002, "Fluidic Self-Assembly of Micromirrors Onto Microactuators using Capillary Forces," IEEE Journal of Selected Topics in Quantum Electronics, 8(1) pg. 4.

[10] Hosokawa, 1994, "Dynamics of Self-Assembling Systems-Analogy with Chemical Kinetics," pg. 172.

[11] Hosokawa, K., 1996, "Two-Dimensional Micro-Self-Assembly using the Surface Tension of Water," Sensors and Actuators.A, Physical, 57(2) pg. 117.

[12] Hongkai, W., 1999, "Selectivities among Capillary Bonds in Mesoscale Self-Assembly," Applied Physics Letters, 75(20) pg. 3222.

[13] Bowden, N., 1999, "Mesoscale Self-Assembly of Hexagonal Plates using Lateral Capillary Forces: Synthesis using the 'Capillary Bond'," Journal of the American Chemical Society, 121(23) pg. 5373.

[14] Wolfe, D., 2003, "Mesoscale Self-Assembly: Capillary Interactions when Positive and Negative Menisci have Similar Amplitudes," Langmuir, 19(6) pg. 2206.

[15] Oliver, S. R. J., Bowden, N., and Whitesides, G. M., 2000, "Self-Assembly of Hexagonal Rod Arrays Based on Capillary Forces," Journal of Colloid and Interface Science, 224(2) pp. 425-428.

[16] D. H., G., M., B., O., O., 2002, "Biomimetic Self-Assembly of Helical Electrical Circuits using Orthogonal Capillary Interactions," Applied Physics Letters, 80 pg. 2802.

[17] Jacobs, H. O., Tao, A. R., Schwartz, A., 2002, "Fabrication of a Cylindrical Display by Patterned Assembly," Science, 296(5566) pp. 323-325.

[18] Mastrangeli, M., 2009, "Self-Assembly from Milli- to Nanoscales: Methods and Applications," Journal of Micromechanics and Microengineering, 19(8) pg. 083001.

[19] Alberty, R. A., and Silbey, R. J., 1992, "Physical chemistry," Wiley, New York.

[20] Ross, S. M., 2003, "Introduction to probability models." Academic Press, San Diego,Calif.

[21] Munson, B. R., Young, D. F., and Okiishi, T. H., 2006, "Fundamentals of fluid mechanics," J. Wiley & Sons, Hoboken, NJ.

[22] Srinivasan, U., 2001, "Microstructure to Substrate Self-Assembly using Capillary Forces," Journal of Microelectromechanical Systems, 10(1) pg. 17.

APPENDICES

Appendix A: Assembly Mount 1 Drawing

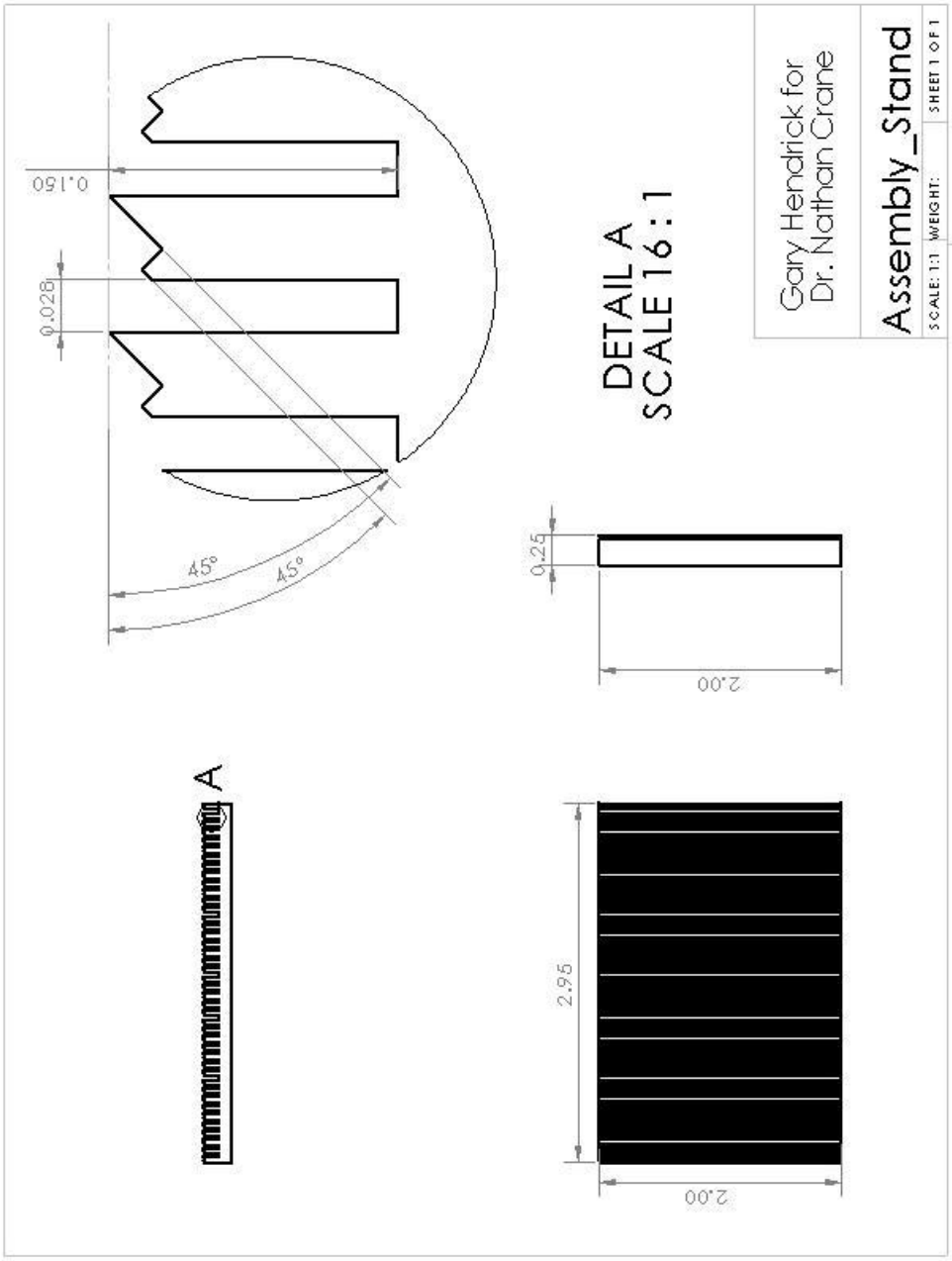

Figure A1: Original assembly mount design. The long milled shelves held assembly sites.

Appendix B: Assembly Mount 2 Drawings

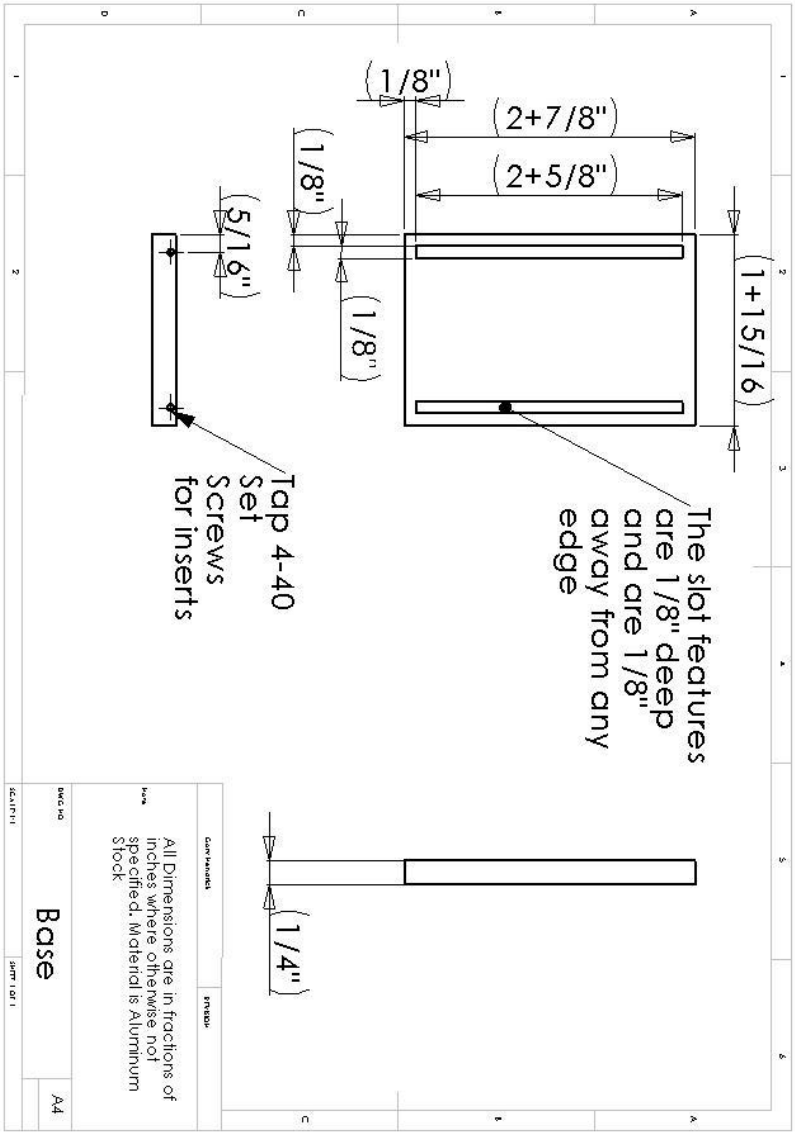

Figure B1: Final design for assembly mount base.

Appendix B (continued)

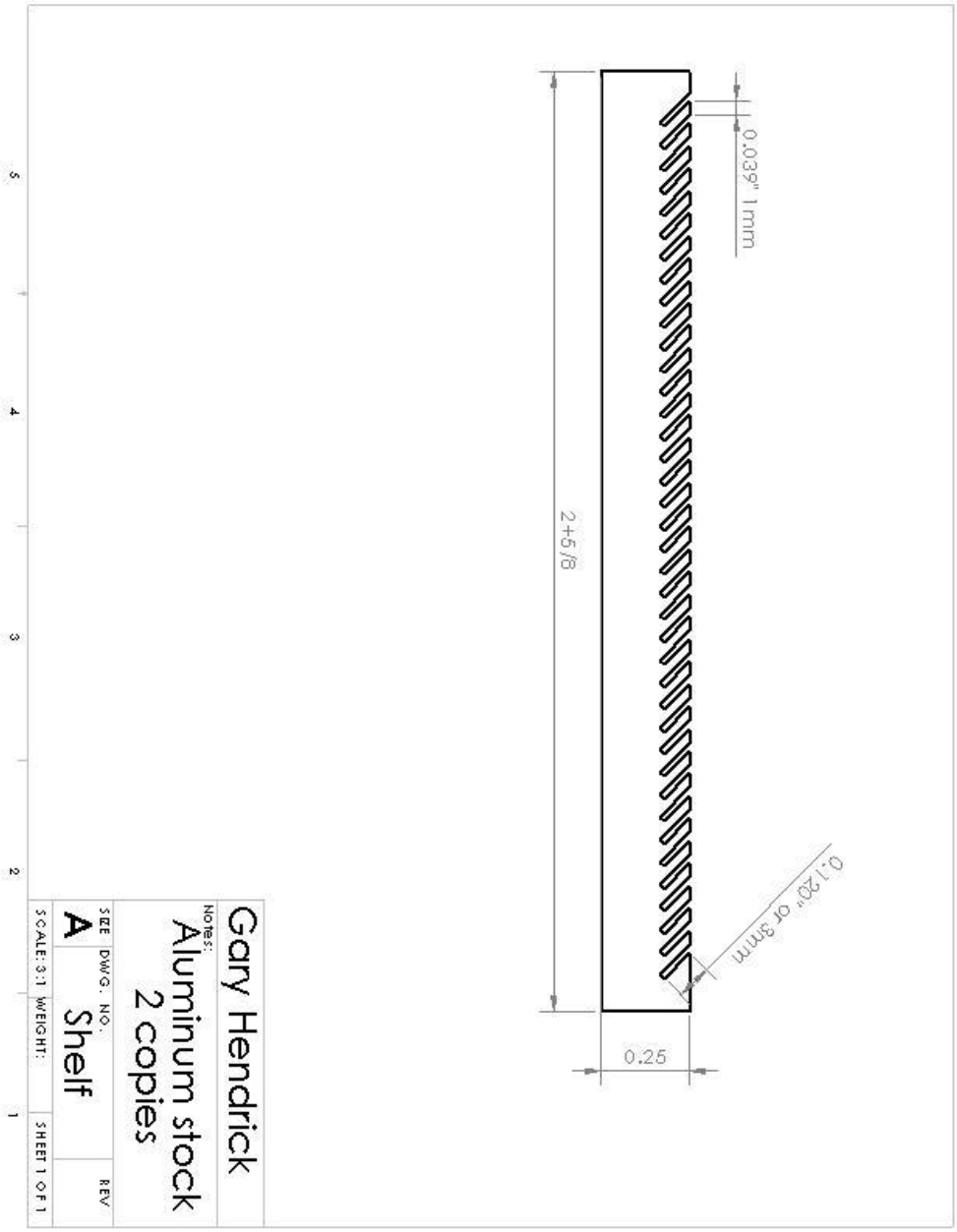

Figure B2: Final design of assembly mount shelves. Two are cut with sawed in slats and finally inserted into the base.

ABOUT THE AUTHOR

Gary Hendrick is a Mechanical Engineering student at the University of South Florida where he received his BSME in 2008 and plans to graduate with his MSME at the summer of 2010. In addition to his research at the micro-scale integration laboratory he has been an active member and leader within the USF chapter of Engineers Without Borders.